

---

---

# Relatório científico - FAPESP

---

---

**Processo:** 2020/04751-4

**Título:** Formação de padrões em recifes de coral

**Beneficiário:** Vivian de Araujo Dornelas Nunes

**Responsável:** Nathan Jacob Berkovits

**Vínculo Institucional:** IFT-UNESP

**Vigência:** 01/08/2020 à 30/11/2022

**Período do relatório:** 01/08/2020 à 30/12/2021

*Vivian de A. D. Nunes*

*Nathan Berkovits*

# 1 Resumo do projeto proposto

Nas últimas décadas muitos pesquisadores tem usado do advento da computação para, através de modelagens matemáticas, entender problemas que não eram tradicionalmente estudados na física. Dentre eles podemos citar a correlação entre uma população e o seu habitat, que é uma questão importante na ecologia e que é abordado também em campos como biologia, matemática e física.

Para descrever a evolução espacial e temporal de uma população de uma determinada espécie, pode-se utilizar um modelo matemático. Desta forma somos capazes de incorporar em uma equação, comportamentos tais como difusão dessa população no ambiente (ou habitat), interação dos seus indivíduos entre indivíduos da mesma espécie ou entre outras espécies, competição por recursos disponíveis, entre outros. Além disso, o modelo escolhido deve ser tal que seja capaz de descrever e de fazer previsões do que vai acontecer nesses sistemas, da forma mais sucinta possível, seja por meio de soluções analíticas, numéricas ou ambas.

O projeto tem como objetivo principal estudar a formação de diferentes tipos de padrões em recifes de corais por meio de modelagem matemática. Ele pode ser desenvolvido levando-se em consideração que os recifes de corais da mesma espécie podem formar diferentes padrões, dependendo das condições ambientais, como fluxo de nutrientes e disponibilidade de luz e água. No decorrer do projeto o tema foi adaptado (devido à oportunidades de colaborações), e veremos a seguir o que já foi estudado e os planejamentos futuros.

## 2 Progresso do projeto

Desde o início do projeto até agora, dois cenários diferentes foram estudados.

O primeiro trabalho leva em consideração o caso em que uma população de uma única espécie habita em um ambiente heterogêneo. Tais condições ambientais são incorporadas no modelo matemático por meio de um coeficiente de difusão dependente do espaço. Neste cenário, estudamos a persistência dessa população e analisamos como essa difusão heterogênea pode reduzir o tamanho do fragmento crítico do habitat, ou seja, o tamanho mínimo que o habitat deve ter, para que permita a sobrevivência da espécie.

No segundo trabalho, está sendo considerada uma população microbiana que vive em um meio fluido. Tal população pode ser composta por dois diferentes fenótipos, onde um deles produz um bem público, com um certo custo associado, que é compartilhado com todos. Analisamos como diferentes tipos de fluxos influenciam na distribuição deste bem público e o papel deles na coexistência dessa população.

## 2.1 O papel da difusão heterogênea na sobrevivência de uma população

Este estudo foi realizado do início do projeto até o mês de outubro de 2020, quando teve sua versão final publicada na PHYSICAL REVIEW E.

### Colaborações:

- Celia Anteneodo (PUC-Rio);
- Maíke A. F. dos Santos (PUC-Rio);
- Eduardo H. Colombo (Universidade de Princeton).

### Motivação:

Algumas espécies vivem em paisagens irregulares nas quais apenas certas regiões fornecem, aos indivíduos, recursos, abrigo e outros ingredientes essenciais para a sobrevivência. Além disso, a fragmentação e degradação do habitat, acelerada pelas atividades humanas, vem produzindo impactos significativos nos ecossistemas, levando muitas espécies à extinção. Portanto, é importante entender como as características espaciais do habitat influenciam na sobrevivência das espécies. Concentrando-se em um único fragmento, um problema importante em ecologia é determinar o tamanho do fragmento crítico para a sobrevivência das espécies.

### Resumo:

Neste trabalho, investigamos o impacto da difusão heterogênea, usando o cálculo de Stratonovich, sobre o tamanho mínimo do fragmento que permite a sobrevivência da população. Combinando simulações numéricas e cálculos analíticos, mostramos que, em geral, esse tamanho crítico é menor que o de

um meio homogêneo com a mesma difusibilidade média. Numericamente, também é possível comparar esse resultado com o do cálculo Itô (que promove o efeito contrário), e com a interpretação de Hänggi-Klimontovich da dinâmica (que reforça esse efeito).

## 2.2 O dilema do bem público em populações microbianas sob um fluxo

Este estudo vem sendo desenvolvido desde o início do projeto e se encontra em andamento. Resultados importantes já foram obtidos e apresentados em congressos. Além disso, um artigo científico está sendo elaborado.

### Colaboração:

- Ricardo Martinez-Garcia (IFT-UNESP / ICTP-SAIFR).

### Motivação:

Bens públicos (PG - Public good) são moléculas produzidas por certos micróbios, que são liberadas no meio ambiente e fornecem um benefício reprodutivo não apenas para os próprios produtores, mas também para outros indivíduos (caronas). Um exemplo de PGs são as enzimas digestivas secretadas por certas bactérias para quebrar polímeros complexos em fontes de carbono mais simples que podem ser importadas e catabolizadas mais facilmente pelas células.

Os ambientes aquosos fornecem um contexto ambiental muito interessante para estudar a produção de PG, pois o fluxo externo propaga microrganismos e as substâncias que eles liberam, e pode gerar dinâmicas muito complexas e inexploradas. O objetivo é entender quais são os mecanismos que tornam a cooperação estável evolutivamente e que explicam por que alguns indivíduos investem parte de sua aptidão individual para fornecer benefícios de aptidão ao coletivo (conhecido como dilema do bem público).

### Resumo:

Neste projeto, estamos interessados em estudar se os fluxos ambientais, que estão presentes em muitos habitats microbianos (rios, lagos, intestinos, pulmões, cavidade nasal...), fornecem uma solução para o dilema do bem

público. Para esse propósito, consideramos uma população bacteriana composta de células produtoras de PG e não produtoras em um biofilme (imerso em um meio aquoso) que modelamos usando um processo estocástico de nascimento-morte. Os bens públicos em nosso modelo são liberados em nós da rede ocupados por células produtoras e livres para flutuar no fluido. Portanto, associamos o processo de nascimento-morte na rede, a uma equação de reação-advectação-difusão para o transporte das moléculas (PGs) em todo o sistema.

Analizamos este modelo para diferentes fluxos a fim de investigar se, e como, a interação entre os fluxos ambientais e os parâmetros fisiológicos poderia tornar a produção de bem público evolutivamente estável. Nossos resultados mostram que os fluxos podem remodelar a distribuição espacial dos bens públicos e fazer com que os produtores de PG e caronas coexistam em condições nas quais o transporte difusivo resultaria na extinção dos produtores de PG.

### 3 Próximas atividades

Referente ao trabalho mencionado na seção 2.2, que está em andamento, temos os seguintes planos:

- Finalizar o artigo e o submeter a uma revista científica;
- Apresentar este trabalho em eventos internacionais, como o *Society of Mathematical Biology 2022 Annual Meeting*;
- Continuar estudando o tema aumentando a complexidade do fluido, incluindo efeitos turbulentos ao modelo;
- Alterar a topologia de distribuição das células na rede, visto que ela tem uma dependência com o tamanho das células, por exemplo;
- Submeter os novos resultados, como um novo artigo, a uma revista científica.

## 4 Participação em eventos científicos

### Conferências

1. Encontro Nacional de Física Estatística (November 22-25, 2021), Online.  
Apresentação oral: *Public good dilemmas under the flow*  
<http://defim.ufsj.edu.br/enfe/enfe.html>
2. Society of Mathematical Biology 2021 Annual Meeting (June 13-17, 2021), Online.  
<https://www.smb2021.org/>
3. Workshop on Limits to Diversity Assembly (January 19-21, 2021), Online.  
<http://indico.ictp.it/event/9511/>
4. XV International Seminar on Biomathematics (September 11-26, 2020), Online.  
<https://sites.google.com/view/xvsembiomat>
5. Society of Mathematical Biology 2020 Annual Meeting (August 17-20, 2020), Online.  
<https://smb2020.org/>

### Mesa redonda

Escola de Verão ICTP-SAIFR para Jovens Físicos (16 a 23 de janeiro, 2021). Tema: *Carreira científica*.

### Bancas de trabalhos de conclusão

Anteneodo, C.; Vieira, A. R.; Ferreira, S. C.; Ramos, M.F. ; Dornelas, V.. Participação em banca de Judson de Oliveira Moura. Controlando o grau médio na construção de redes complexas. 2021. Dissertação (Mestrado em Física) - PUC-Rio.

## 5 Lista de publicações

DOS SANTOS, M. A. F. ; DORNELAS, V. ; COLOMBO, E. H. ; ANTE-NEODO, C. Critical patch size reduction by heterogeneous diffusion. PHYSICAL REVIEW E, v. 102, p. 042139, (2020).

**Critical patch size reduction by heterogeneous diffusion**M. A. F. dos Santos <sup>1</sup>, V. Dornelas <sup>1,2</sup>, E. H. Colombo <sup>3,4</sup> and C. Anteneodo <sup>1,5</sup><sup>1</sup>*Department of Physics, PUC-Rio, Rua Marquês de São Vicente 225, 22451-900, Rio de Janeiro, RJ, Brazil*<sup>2</sup>*ICTP-SAIIR & IFT-UNESP, Rua Dr. Bento Teobaldo Ferraz 271, 01140-070, São Paulo, SP, Brazil*<sup>3</sup>*Department of Ecology & Evolutionary Biology, Princeton University, Princeton, New Jersey 08544, USA*<sup>4</sup>*Department of Ecology, Evolution, and Natural Resources, Rutgers University, New Brunswick, New Jersey 08901, USA*<sup>5</sup>*Institute of Science and Technology for Complex Systems (INCT-SC), Rio de Janeiro, Brazil* (Received 6 August 2020; revised 6 October 2020; accepted 13 October 2020; published 29 October 2020)

Population survival depends on a large set of factors and on how they are distributed in space. Due to landscape heterogeneity, species can occupy particular regions that provide the ideal scenario for development, working as a refuge from harmful environmental conditions. Survival occurs if population growth overcomes the losses caused by adventurous individuals that cross the patch edge. In this work, we consider a single species dynamics in a patch with a space-dependent diffusion coefficient. We show analytically, within the Stratonovich framework, that heterogeneous diffusion reduces the minimal patch size for population survival when contrasted with the homogeneous case with the same average diffusivity. Furthermore, this result is robust regardless of the particular choice of the diffusion coefficient profile. We also discuss how this picture changes beyond the Stratonovich framework. Particularly, the Itô case, which is nonanticipative, can promote the opposite effect, while Hänggi-Klimontovich interpretation reinforces the reduction effect.

DOI: [10.1103/PhysRevE.102.042139](https://doi.org/10.1103/PhysRevE.102.042139)**I. INTRODUCTION**

Species typically experience a patchy landscape, where only within certain regions individuals can find resources, shelter, and other key ingredients for survival [1]. The landscape spatial structure shapes diverse macroscopic ecological patterns, affecting, for instance, the stability and diversity of ecosystems [2,3]. Particularly, the fragmentation and degradation of the habitats, accelerated by human activities, have been producing significant impacts on ecosystems, leading many species to extinction [4,5]. Thus, it is, more than ever, a matter of interest to understand the role that habitat spatial features exert on species survival.

Focusing on a single patch, a central problem is to determine the critical patch size for species survival. Typically, there exists a minimum size  $L_c$  that separates the extinction and survival regimes. Then, if the patch size  $L$  is bigger than  $L_c$ , the population can grow, achieving a stationary profile at long time, while it goes extinct otherwise. The specific value of  $L_c$  depends on the details of the environment and population dynamics.

Pioneer investigations have addressed species survival assuming a time-independent bounded habitat and that individuals diffuse and reproduce with constant rates [6–8]. More recently, theoretical developments have been made to include demographic fluctuations, which arise from the stochastic character of the birth-death process [9], and experimental realization using specific strains of bacteria was performed to check the validity of the theory [10]. Beyond this classical case, previous works have discussed the effect of the spatiotemporal structure of the environment [11–15], advection [16,17], chemotaxis [18], and nonlinear response [19]. These

features can affect the value of  $L_c$ , as they substantially modify the flux of individuals through the habitat edge [20,21]. Furthermore, it has been shown that the common sense that larger patches favor species survival breaks down if a strong nonlinearity is present [19]. Similarly, in the multispecies context, it has been shown that small patches can have high conservation value [22,23].

Despite previous works have already tackled the critical patch size problem from many different perspectives, the effect of the space-dependent diffusion coefficient has not been sufficiently addressed. Several mechanisms can make the diffusion coefficient depend on the particular location inside the patch. For instance, the composition and structure of the medium through which individuals move can change, facilitating, or hindering, their mobility. This is characteristic of transition zones (ecotones) between habitat and nonhabitat regions which can distort animal movement [24,25]. Also, behavioral responses can affect mobility, as when individuals perceive at a distance [26] the drastic change in the environmental conditions near the edge of the habitat [21,27–30]. Regardless of the mechanisms that regulate the spatially dependent diffusion coefficient, heterogeneity would affect the residence time of the organisms in the patch [31], thus impacting the critical patch size.

The role of space-dependent diffusion on the critical patch size has been studied before in simplified settings, assuming an abrupt change close to the edge of the patch [32,33]. In this work, we extend this investigation for the case where the diffusion coefficient within the patch has a general form.

We consider a single species that grows and moves in a bounded domain, with diffusivity that varies in space. At the

---

# Scientific Report

---

Title	Machine Learning techniques applied to Cosmological Problems
Postdoc	Martin Emilio de los Rios
Supervisor	Nathan Berkovits
FAPESP process	2019/08852-2
Reporting period	1/06/2019 to 30/05/2021

*Nathan Berkovits*



*Martin Emilio de los Rios*

## 1 Original proposal

Machine learning techniques represents a new way of analyzing big data-sets in an agnostic and homogeneous way. These methods are very useful and powerful tolls to find patterns and relations between the variables that are involved in a specific problem. It is worth to mention that these techniques have been applied with a lot of success in technological problems and in other scientific areas, including astronomy and physics. On the other hand, current and future astronomic surveys will generate enormous amount of information, making the machine learning techniques important tools for their analysis. During this postdoc I will applied this new techniques to different cosmological problems. Specifically, I will improve the machine learning algorithms for the automatic classification of merging clusters, in order to applied it for high-redshift and Sunyaev-Zeldovich clusters. At the same time I will continue studying in an individual way the merging clusters candidates found previously. I also will continue the studies of the cosmic microwave background anisotropies with the aim of find if there are any signal of the departure from the standard cosmological model. Specifically I will apply anomaly detection algorithms to find zones of the sky which may present deviations from what it is expected.

## 2 Research.

- **Estimation of dark matter in spiral galaxies:**

*In collaboration with Prof. Fabio Iocco and the Dark Machines Collaboration*

*Status: We are writing a draft with the preliminary results and planning to submit it for its publication to an international journal by the end of the first semester of 2021.*

The main goal of this project is to estimate the dark matter distribution in spiral galaxies using deep learning techniques applied to galaxy photometric images and galaxy gas velocity field maps.

During the first part of this project we analyzed the Illustris TNG hidrodynamical cosmological simulation [7]. Using this simulation we build a data-set composed by synthetic photometric images and velocity field maps of thousands of galaxies. In order to have a representative data-set that resembles real observations, we included all the relevant observational effects (resolution effects of the telescope, shot noise and spread in the inclinations and distances of the galaxies).

Using this data-set we trained and tested several deep learning models to estimate the dark matter distribution of each galaxy. We achieved a precision of  $\approx 20\%$  in all the relevant radii for the galaxies of the test set.

In a second stage of the project we will compare our results with the results obtained by applying the traditional rotation curve technique.

At a final stage of this project we will apply our deep learning methods to real images in order to found their dark matter profiles.

At the present moment we are writing a draft with the first results of the project and planning to submit it by the end of the current semester.

- **Deep learning analysis of strong lensing images.**

*In collaboration with Prof. Rogerio Rosenfeld and researchers from the LSST collaboration.*

*Status: We are writing a draft with the preliminary results and planning to submit it for its publication to an international journal at the second semester of 2021.*

The standard cosmological model with a cold dark matter component predicts several dark substructures with masses bellow  $10^8 M_\odot$  that are not heavy enough to maintain the necessary

gas to form stars, and hence they can only be detected through their gravitational effects. Strong lensing images are one of the most interesting observables where to look for the signal of such subhalo population.

In this project we created a synthetic dataset of strong lensing images using the `deeplenstronomy` code [6]. As different dark matter particles will imply different dark matter subhalo population, we create synthetic images varying the lower-mass cut-off of such population. In order to understand how the different observational effects affect the performance of the methods, we create several data-set including different degree of realism and different observational effects.

Using these data-sets we are exploring the possibility of measuring the minimum mass cut-off with deep learning techniques. Specifically we developed several deep learning methods that has as input different number of staked strong lensing images. We found that, as expected, when increasing the number of stacked images the performance of the method increase.

- **Machine learning analysis of the Cosmic Microwave Background:**

*In collaboration with Prof. Rogério Rosenfeld & Dr. Antonino Troja*

*Status: I recently submit a paper with the results of the first stage of the project to the international journal Monthly Notices of the Royal Astronomical Society.*

The main goal of this project is to analyze the cosmic microwave background with machine learning techniques.

Specifically I developed an auto-encoder (neural network with a bottle-neck layer) [4] with a custom loss function that ensure the physical interpretation of the latent-space variables. The advantage of such method is two-fof. On one hand, the encoder can be used to estimate the cosmological parameters that best fits a given cosmic microwave power spectrum. On the other hand, the decoder can be used to estimate the power spectrum from a given set of cosmological parameters. It is worth to remark that the decoder can also be used as a forward model to estimate the full-posterior probability of the cosmological parameters through a Bayesian analysis in a much faster way than using traditional methods as CAMB or CLASS. The results found in this project were recently submitted for their publication to the international journal *Monthly Notices of the Royal Astronomical Society*. I also created a public available python package were any user can used the pre-trained auto-encoder to analyze CMB data. This code can be downloaded and installed from my personal [github repository](#).

Is customary in CMB analysis to introduce a mask in order to remove foreground sources of contamination. As it is a well-known problem, this mask introduces deviations on the correlation functions that must be taken into account before any statistical analysis. At the moment it is common to use the code `NAMASTER` [1] to remove the deviations introduced by the mask in the Power spectrum (Fourier transform of the 2-point correlation function). Nevertheless this code is not able to remove the deviations introduced on higher-order correlation functions. Taking advantage of the flexibility of machine learning models, at a second stage of this project we will apply denoising machine learning techniques in order to remove the signal introduced by the mask on 2-point and 3-point correlation functions and their corresponding Fourier transform.

In this moment we are creating the necessary data-set that we will use to train and test the denoising techniques. In order to do this we are using the techniques previously developed by Dr. Antonino Troja to compute the power spectrum and bi-spectrum of the CMB.

- **Back-splash galaxies classification:**

*In collaboration with researchers from IATE-UNC (Argentina), Universidad la Serena (Chile) and UNLP (Argentina).*

*Status: We published a paper with the first results of the project in the international journal Monthly Notices of the Royal Astronomical Society [3].*

The main goal of this project is to identify back-splash galaxies in the projected phase-space (distance to the cluster vs relative line-of-sight velocity between the galaxy and the cluster). Specifically we build a data-set of simulated galaxies using the semi-analytical model developed by *Cora et al.* [2] applied to the Multi-Dark cosmological simulations [5]. We classify each simulated galaxy by studying their real 3D orbits around their corresponding cluster. After that, we used the data-set to train different machine learning methods to find the real 3D classification from the observational projected phase-space.

We found that the best performance was achieved by the K-Nearest Neighbor algorithm with better results than the obtained using traditional methods.

This project gave place to a paper that was published on the international journal *Monthly Notices of the Royal Astronomical Society* [3], and to a public code that it is available in my [github repository](#).

It is also important to remark that the ROGER software, originally designed as an R package, will be soon available as a python package and will be part of a more general python environment specifically designed for the analysis of extragalactic data, from which I am the main contributor.

In a second stage of this project we are analysing the properties of the different types of galaxies and how they evolve in cosmological simulations. We are also analysing the properties of the different types of galaxies in several real clusters. This will allow us to compare the properties of real galaxies with the simulated ones. This, in turn, will improve our understanding on how different environments affect the galaxy properties and how reliable are cosmological simulations to model these effects.

- **Merging Clusters Identification:**

*Status:* We are translating all the codes to the python language and developing a full environment for the analysis of extragalactic data.

In this project I build a new R package that is publicly available through my github repository [4]. This package is an implementation of the method that I developed during my PhD for the automatic identification of merging clusters. Also, at the present moment I am working on the translation of the R package to python. This new python package will be part of a bigger python environment specifically designed for the analysis of extragalactic data, from which I am the main contributor.

### 3 Conferences and seminars.

- The dark side of the Universe. From 15/07/2019 to 19/07/2019. (Buenos Aires-Argentina)
- III Joint ICTP Trieste-ICTP-SAI FR School on observational cosmology. From 22/07/2019 to 02/08/2019. ICTP-SAI FR (Sao Paulo-Brazil).
- School on High Energy Astrophysics. From 05/08/2019 to 16/08/2019. ICTP-SAI FR (Sao Paulo-Brazil).
- Linea Bootcamp. From 02/09/2019 to 06/09/2019. Observatório Nacional (Rio de Janeiro-Brazil).
- Dark Universe Workshop – Early Universe Cosmology, Baryogenesis and Dark Matter. From 21/10/2019 to 25/10/2019. ICTP-SAI FR (Sao Paulo-Brazil).
- 62° Annual Meeting of the Argentinian Astronomy Society. **Oral Contribution.** From 13/10/2020 to 16/10/2020. Rosario-Argentina (by Videoconference).

---

<sup>1</sup><https://github.com/Martindelososrios/MeSsl>

- Deep Learning for Science School. from 07/2020 to 09/2020. Lawrence Berkeley National Laboratory (by Videoconference).
- II Joint Trieste/SAIFR School on Particle Physics. From 22/06/2019 to 02/07/2019. ICTP-SAIFR. Sao Paulo-Brazil (by Videoconference).
- First School on Data Science and Machine Learning. From 16/12/2019 to 20/12/2019. ICTP-SAIFR (Sao Paulo-Brazil).
- 2nd Latin American School on Parallel Programming for High Performance Computing. From 02/12/2019 to 13/12/2019. ICTP-SAIFR (Sao Paulo-Brazil).
- 62° Annual Meeting of the Argentinian Astronomy Society. **Oral Contribution.** From 13/10/2020 to 16/10/2020. Argentina.
- 3<sup>rd</sup> South American Dark Matter Workshop. From 02/12/2020 to 04/12/2020. ICTP-SAIFR (Sao Paulo-Brazil).
- Workshop on New Trends in Dark Matter. From 07/12/2020 to 09/12/2020. ICTP-SAIFR (Sao Paulo-Brazil).
- Latin American Workshop on Observational Cosmology. From 14/12/2020 to 18/12/2020. ICTP-SAIFR (Sao Paulo-Brazil).
- XI FOF Meeting. From 26/04/2021 to 30/04/2021. IATE-UNC (Córdoba-Argentina).

## 4 Other Activities.

During the two years that I spend as a postdoc fellow at ICTP-SAIFR/IFT-UNESP I organized the weekly Journal Club on Cosmology and Astrophysics.

## References

- [1] David Alonso, Javier Sanchez, Anže Slosar, and LSST Dark Energy Science Collaboration. A unified pseudo- $C_\ell$  framework. *Monthly Notices of the Royal Astronomical Society*, 484(3):4127–4151, April 2019.
- [2] Sofía A Cora, Cristian A Vega-Martínez, Tomás Hough, Andrés N Ruiz, Álvaro A Orsi, Alejandra M Muñoz Arancibia, Ignacio D Gargiulo, Florencia Collacchioni, Nelson D Padilla, Stefan Gottlöber, and Gustavo Yepes. Semi-analytic galaxies – I. Synthesis of environmental and star-forming regulation mechanisms. *Monthly Notices of the Royal Astronomical Society*, 479(1):2–24, 05 2018.
- [3] Martín de los Rios, Héctor J. Martínez, Valeria Coenda, Hernán Muriel, Andrés N. Ruiz, Cristian A. Vega-Martínez, and Sofía A. Cora. ROGER: Reconstructing orbits of galaxies in extreme regions using machine learning techniques. *Monthly Notices of the Royal Astronomical Society*, 500(2):1784–1794, January 2021.
- [4] G. E. Hinton and R. R. Salakhutdinov. Reducing the dimensionality of data with neural networks. *Science*, 313(5786):504–507, 2006.
- [5] Alexander Knebe, Doris Stoppacher, Francisco Prada, Christoph Behrens, Andrew Benson, Sofia A Cora, Darren J Croton, Nelson D Padilla, Andrés N Ruiz, Manodeep Sinha, Adam R H Stevens, Cristian A Vega-Martínez, Peter Behroozi, Violeta Gonzalez-Perez, Stefan Gottlöber, Anatoly A Klypin, Gustavo Yepes, Harry Enke, Noam I Libeskind, Kristin Riebe, and Matthias Steinmetz.

- MultiDark-Galaxies: data release and first results. *Monthly Notices of the Royal Astronomical Society*, 474(4):5206–5231, 10 2017.
- [6] Robert Morgan, Brian Nord, Simon Birrer, Joshua Yao-Yu Lin, and Jason Poh. deepenstronomy: A dataset simulation package for strong gravitational lensing. *Journal of Open Source Software*, 6(58):2854, 2021.
- [7] Volker Springel, Rüdiger Pakmor, Annalisa Pillepich, Rainer Weinberger, Dylan Nelson, Lars Hernquist, Mark Vogelsberger, Shy Genel, Paul Torrey, Federico Marinacci, and Jill Naiman. First results from the IllustrisTNG simulations: matter and galaxy clustering. *Monthly Notices of the Royal Astronomical Society*, 475(1):676–698, March 2018.



**ICTP** | International Centre for Theoretical Physics  
**SAIFR** | South American Institute for Fundamental Research

## Scientific Report 2021

### Movement strategies and population dynamics in heterogeneous environments

---

Postdoctoral Fellow: Gabriel Andreguetto Maciel *Gabriel A. Maciel*

Supervisor: Nathan Jacob Berkovits

*Nathan Berkovits*

Fapesp process: 2019/21227-0

Project duration: 01/Jan/2020 - 30/Nov/2022

Report period: 01/Jan/2020 - 30/Dec/2021

---

## Abstract

The initial aim of this project was to study movement strategies and their effects on the dynamics of populations in heterogeneous environments. The first year of execution, as mentioned in the previous report, was devoted to the study of two competing populations that interact non-locally. That work has been published in the Journal of Theoretical Biology ([Maciel and Martinez-Garcia, 2021](#)). In this second year we have focused on the effects of belowground interactions on the growth of plant roots. We have extended previous models to include effects of plant engineering and investigate the emergence of facilitation phenomena. We explored the effects of engineering on the growth of roots of a single plant and obtained conditions where an engineer plant can facilitate another plant. We are finishing calculations and we already started writing an article about this project.

# 1 Activities from 01/Dec/2020 - 30/Dec/2021

## 1.1 The evolutionary dilemma of antagonistic facilitation in plants

### 1.1.1 Overview

Plants employ a wide variety of strategies to access belowground resources. Despite great advances in recent years, there are still several open questions about the dynamics of roots growth and interactions. These gaps in our understanding are partially due to the difficulties in studying the dynamics belowground.

[Cabal et al. \(2020\)](#) used a game theoretical model and experiments to study the dynamics of roots growth and allocation of species that exploit a shared resource. We extended that purely exploitation model to include effects of plant engineering ([Hastings et al., 2007](#)). In a broad sense, plant engineers are species that can modify the environment, potentially changing growth and survival conditions. One remarkable example of plant engineering is the hydraulic lift performed by some plants, where specialized roots pump water from deeper soil to the surface ([Ludwig et al., 2004](#)). In one hand, engineering increases resources available for the plants but in the other it can increase competitors population in addition to extra costs for the engineer. This poses a dilemma where facilitation does not seem advantageous for the benefactor while it is still reported in several biological systems. In this work we study the effects of engineering on the dynamics of two interacting plants.

### 1.1.2 Single plant model

We initially consider a single plant engineer that feeds on a given resource. Root and resource biomass densities are denoted, respectively, by  $R(x, t)$  and  $W(x, t)$ ,

where  $x$  and  $t$  are the spatial location and time. Resource dynamics is then given by the balance between the input rate in the system, natural decaying rate and plant consumption. As the engineer potentially modifies the resource availability in the system we write the input rate as  $I(R(x, t))$ . Accordingly, resource dynamics in our model are governed by the equation:

$$\frac{\partial W(x, t)}{\partial t} = I(R(x, t)) - \delta W(x, t) - \alpha R(x, t)W(x, t), \quad (1)$$

where  $\delta$  is the resource natural decaying rate and  $\alpha$  is the rate in which resource is consumed by the roots.

We further assume the resource that becomes available for the plant is a fraction of the environment input rate  $w$  and engineering increases the fraction that the plant can have access to. We thus write the input rate function  $I(R(x, t))$  as:

$$I(R(x, t)) = w \left( \frac{b + \phi R(x, t)}{1 + \phi R(x, t)} \right). \quad (2)$$

The constant  $b$  gives the fraction of  $w$  that becomes available resource when there is no engineering ( $\phi = 0$ ). The input fraction increases with the root density as a result of engineering and saturates at 1 for large  $R$ , where the plant has access to the full intake  $w$ . Parameter  $\phi$  determines how fast the input increases and therefore controls the engineering potential.

We now write the fitness-generating function for the plant as the difference between the gain from resource consumption and the costs of growing roots:

$$G(x, t) = [Q\alpha W(x, t) - C(x)] R(x, t), \quad (3)$$

where  $Q$  is the conversion factor and  $C(x)$  accounts for costs related fitness reduction. The cost per biomass is a sum of a constant cost associated to the growth of fine roots, a cost term that increases with distance from the insertion point and an extra cost associated with the engineering. Assuming the insertion point is at the origin, we write:

$$C(x) = C_b + C_t x^2 + C_e \phi. \quad (4)$$

We assume the resource dynamics occurs at a much faster time scale than the roots growth. Therefore, resource is always at the equilibrium:

$$W(x, t) = \frac{I(R(x, t))}{\delta + \alpha R(x, t)}. \quad (5)$$

Inserting this expression in the fitness-generating function (3) we can finally write:

$$G(x, t) = \left[ Qa \frac{b + \phi R}{1 + \phi R} - (C_b + C_t x^2 + C_e \phi) \right] R(x, t), \quad (6)$$

where we have used the rescaling  $a = \alpha/\delta$ .

### 1.1.3 Evolutionarily stable strategies (ESS) of a single plant

We look for the ESS in this system by maximizing the fitness-generating function in two different scenarios. In the first scenario we look for the root allocation distribution that maximizes  $G(x, t)$  and assume that the engineering parameter  $\phi$  is a given established constant. In the second scenario we consider  $\phi$  is trait subject to evolution and thus  $G(x)$  is maximized in terms of both  $\phi$  and  $R(x)$ .

*$\phi$  as a given constant*

In this scenario we simply look for the root distribution  $R(x)$  that maximizes  $G(x)$  by comparing the interior maxima at the critical points:

$$\frac{\partial G}{\partial R} = 0 \quad (7)$$

with the trivial state  $R = 0$ , corresponding to  $G(x) = 0$ . From (7) we obtain necessary and sufficient conditions for the existence of real and positive root distributions at critical points. First, positive interior points exist only if:

$$\omega Qa > C_b + C_t x^2 + C_e \phi, \quad (8)$$

which somehow represents the fact that the plants gain needs to be higher than the total cost. Sufficient conditions can be further obtained. Here, we need either:

$$b > \frac{C_b + C_t x^2 + C_e \phi}{\omega Qa} \quad (9)$$

or

$$C_e < \frac{\gamma}{a} \quad \text{and} \quad \phi^- < \phi < \phi^+, \quad (10)$$

where:

$$\gamma = \omega Qa - (C_b + C_t x^2) \quad \text{and} \quad \phi^\pm = \frac{\gamma - aC_e}{2C_e} \left( 1 \pm \sqrt{1 - \frac{4a(C_b + C_t x^2)C_e}{(\gamma - aC_e)^2}} \right). \quad (11)$$

We notice, however, that while above expressions guarantee the existence of interior critical points with  $R(x) > 0$  in some cases they are associated with negative

fitness and therefore these strategies are not better than the trivial one  $R(x) = 0$ . But still these conditions allow us to derive important insights from this single plant system. The plant is sustained either through a sufficient basal intake fraction  $b$  or if engineering cost is low and the engineering constant assumes intermediate values, as expressed in conditions (9) and (10) respectively. Thus, engineering can sustain the plant if it is not too low, in which case it does not increase the resource to sufficient levels, and it is not too large as to impose too high a cost.

Figure 1 shows examples of root distributions at the ESS. In panel (a) we set parameters so that only (9) is satisfied while in panel (b) only (10) holds. The two distributions have striking and interesting qualitative differences. When the plant is sustained by the engineering there is a discontinuous jump in density which appears because plant is maintained only in locations where densities are high enough for the engineering to be sufficiently high.

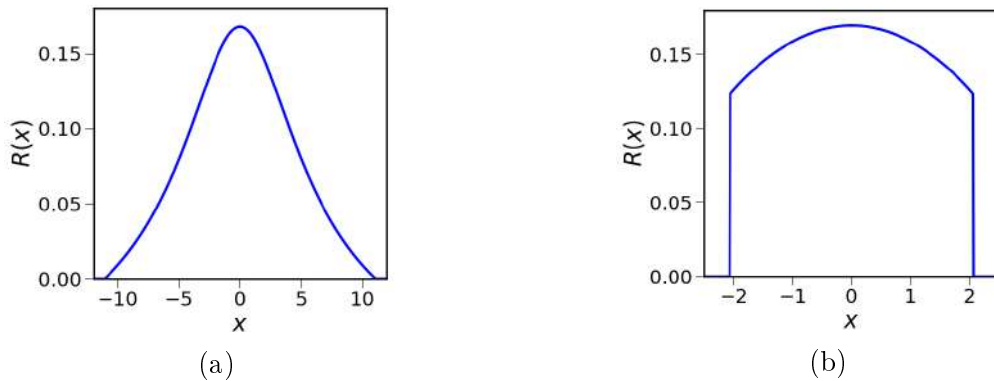


Figure 1: Root spatial distributions. In (a) only condition (9) is satisfied while in (b) only the inequality in (10) holds.

#### *$\phi$ as a trait subject to evolution*

In this second scenario we assume  $\phi$  is a trait subject to evolution and therefore the ESS involves maximizing  $G(x, t)$  with respect to both  $R(x)$  and  $\phi$ . I show here the case where the value of parameter  $\phi$  evolves but it is assumed spatially constant. Here, the ESS is obtained by first fixing the value of  $\phi$  and then looking for  $R(x)$  that maximizes  $G(x)$  using (7). We repeat this process for different values of  $\phi$  and obtain the ESS as the strategy that maximizes the total fitness  $\int G(x)dx$ . At the ESS we then obtain distributions qualitatively similar to those in Figure 1.

### 1.1.4 Two plants model

For the two plants model we write root densities as  $R_1(x)$  and  $R_2(x)$ . Assuming only species 1 is an engineer, now the resource growth dynamics are governed by the equation:

$$\frac{\partial W(x, t)}{\partial t} = \omega \frac{b + \phi R_1(x, t)}{1 + \phi R_1(x, t)} - \delta W(x, t) - \alpha_1 R_1(x, t) W(x, t) - \alpha_2 R_2(x, t) W(x, t). \quad (12)$$

And for two plants at a distance  $d$  apart the fitness-generating functions for the two plants read:

$$G_1(x, t) = [Q_1 \alpha_1 W(x, t) - (C_{b1} + C_{t1} x^2 + C_e \phi)] R_1(x, t) \quad (13)$$

$$G_2(x, t) = [Q_2 \alpha_2 W(x, t) - (C_{b2} + C_{t2} (x - d)^2)] R_2(x, t). \quad (14)$$

Parameters have the same meaning as in the single plant scenario except that now we make them species specific. Again we assume the resource is at equilibrium and write:

$$G_1(x, t) = \left[ Q_1 a_1 \frac{\frac{b + \phi R_1}{1 + \phi R_1}}{1 + a_1 R_1 + a_2 R_2} - (C_{b1} + C_{t1} x^2 + C_e \phi) \right] R_1(x, t) \quad (15)$$

$$G_2(x, t) = \left[ Q_2 a_2 \frac{\frac{b + \phi R_1}{1 + \phi R_1}}{1 + a_1 R_1 + a_2 R_2} - (C_{b2} + C_{t2} (x - d)^2) \right] R_2(x, t). \quad (16)$$

The ESS in this two plants game is obtained by maximizing  $G_1$  in terms of species 1 strategies, i.e. in terms of roots distribution,  $R_1(x)$ , and engineering strength,  $\phi$ , and maximizing  $G_2$  in terms of species 2 roots distribution,  $R_2(x)$ . As before, we fix  $\phi$  at a given constant value and look for interior maxima at the critical points from:

$$\frac{\partial G_1}{\partial R_1} = 0 \quad \text{and} \quad \frac{\partial G_2}{\partial R_2} = 0. \quad (17)$$

Repeating the calculations for different values of  $\phi$ , the interior maximum is given by the strategy that maximizes the total fitness of species 1,  $\int G_1(x) dx$ . The global maxima, and therefore the ESS, is obtained by comparing the interior points with the no engineering strategy,  $\phi = 0$ .

In Figure 2, we choose parameters so that both species can sustain themselves in the environment independently of engineering ( $b > C_{b1}/(\omega Q_1 a_1)$  and  $b > C_{b2}/(\omega Q_2 a_2)$ ). Although the two species coexist, we have compared the total fitness of the oppor-

tunist species (species 2) in the presence of the engineer and when alone and we found its fitness in fact decreases when species 1 is present. Thus in this case, competition for resources is greater than the potential facilitative effect of species 1 on 2.

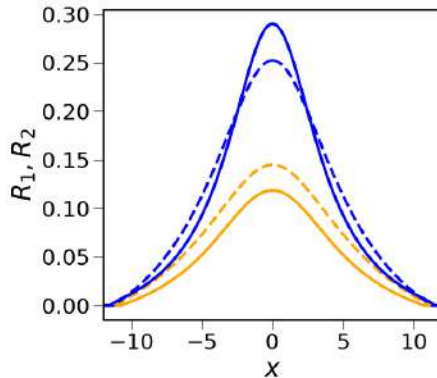


Figure 2: Root distributions at the ESS. Solid blue and orange curves give distributions for the species 1 and 2, respectively. Dashed blue and orange lines are the single plant distributions of species 1 and 2. Parameters are:  $\omega = 5$  ,  $Q_1 = 1$  ,  $a_1 = 10$  ,  $Q_2 = 1$ ,  $a_2 = 10$  ,  $C_{b1} = 3$  ,  $C_{t1} = 0.2$ ,  $C_{b2} = 5$  ,  $C_{t2} = 0.2$ ,  $b = 0.6$ .  $\phi = 0.65$  (solid lines) and  $\phi = 3$  (dashed blue line)

When the environment does not sustain any of the two plant species in the absence of engineering ( $b < C_{b1}/(\omega Q_1 a_1)$  and  $b < C_{b2}/(\omega Q_2 a_2)$ ) we find that engineering not only allows the engineer species to survive but also provides conditions for the establishment of the opportunist species, as shown in Figure 3. We have found therefore a case of two species that exploit a common resource but where one of them facilitates the growth of the other. This situation has been termed antagonistic facilitation.

## 2 Activities from 01/Jan/2020 - 30/Nov/2020

### 2.1 How spatial self-organization enables coexistence of two competing species

Competition is a widespread phenomenon with critical consequences for the composition of ecosystems. A common conclusion of early mathematical models, though, is that the coexistence between competing species is impossible or restricted to weak interactions. In order to understand how these apparently highly unstable systems are so ubiquitous in nature, in the past few decades a vast wealth of studies have

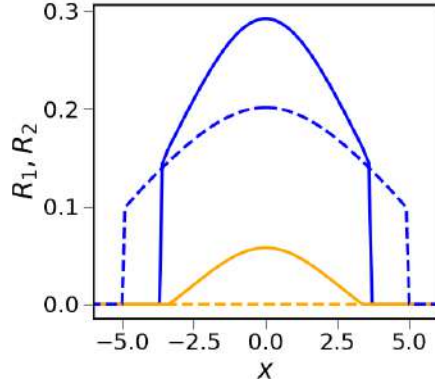


Figure 3: Root distributions at the ESS. Curves colors and patters follow those of Figure 2. We have  $b = 0.05$ ,  $\phi = 3.3$  (solid lines) and  $\phi = 8.5$  (dashed blue line). Other parameters are as in Figure 2.

looked for mechanisms present in real populations that could facilitate the coexistence of competing species. In this work we have explored in detail a coexistence mechanism based on the spatial self-organization of the populations.

We studied the dynamics of competition between two species that can interact locally and non-locally. Population dynamics were studied through kernel-based models, which are known to induce non-uniform distribution patterns of single species. Thus, denoting population densities of the two competitors at time  $t > 0$  and position  $x \in \mathbb{R}$  by  $\rho_1(x, t)$  and  $\rho_2(x, t)$ , population dynamics are governed by the integrodifferential equations:

$$\frac{\partial \rho_1}{\partial t} = D_1 \frac{\partial^2 \rho_1}{\partial x^2} + b_1 \rho_1 \left( 1 - \frac{\rho_1 + a_{12} \rho_2}{K_1} \right) - \left( \delta_1 \int G_{11}(|x - x'|) \rho_1(x', t) dx' + h_1 \int G_{12}(|x - x'|) \rho_2(x', t) dx' \right) \rho_1 \quad (18)$$

$$\frac{\partial \rho_2}{\partial t} = D_2 \frac{\partial^2 \rho_2}{\partial x^2} + b_2 \rho_2 \left( 1 - \frac{\rho_2 + a_{21} \rho_1}{K_2} \right) - \left( \delta_2 \int G_{22}(|x - x'|) \rho_2(x', t) dx' + h_2 \int G_{21}(|x - x'|) \rho_1(x', t) dx' \right) \rho_2, \quad (19)$$

where  $b_i$  and  $K_i$  are, respectively, the growth rate and carrying capacity of species  $i = \{1, 2\}$ .  $a_{12}$  and  $a_{21}$  are the coefficients of local interspecific competition as in the classical Lotka-Volterra model. The coefficients  $\delta_i$  and  $h_i$  control the effects of non-local intra and interspecific competition, respectively. Finally,  $D_1$  and  $D_2$  are the diffusivities and the kernel function  $G_{ij}$  weighs the impact of species  $j$  on species  $i$  at different distances from central locations.

We have combined analytical and numerical techniques in the analysis of the above equations. Our results show that nonlocal interactions can lead to a rich variety of nonuniform distributions in two species competition systems. The self-organized patterns can exhibit, for example, in phase oscillations of coexisting competitors when local competition is weak and anti-phase oscillations otherwise. Most notably, the species coexist under conditions where competitive exclusion occurs in the usual local model. Coexistence here is manifested through a mechanism that involves the weaker competitor being able to explore areas where the stronger competitor population is sparse.

We are finalizing an article about this project and we might have it submitted to a scientific journal soon. I have also presented this work in a short talk on the annual meeting of the Society of Mathematical Biology.

## 3 Future activities

### 3.1 Closing the antagonistic facilitation project

We plan to carry further calculations to explore conditions where facilitation arises in our model of two plants. One interesting aspect we will investigate is how the system behaves along a stress gradient in the environment. A very common stated hypothesis is that facilitation should happen in more stressed environments ([Dohn et al., 2013](#)). In our model, parameters  $\omega$ ,  $b$  and  $\delta$  represent different types of environmental stress (such as reduced raining, decreased soil productivity, and so on) and the system dependence on these parameters will be initially tested.

### 3.2 Applications in agriculture

This project can be extended to other very interesting investigations. There are applications, for example, on agriculture that we would like to work on. For instance, facilitation could be explored to provide greater yields of a given culture. One setting that has been applied to increase productivity is the alternation of different cultures where one of the species potentially facilitates the growth of the other ([Hauggaard-Nielsen and Jensen, 2005](#)). We could use our results to find optimum settings in such cases.

## 4 Participation in scientific events

In August 17-20, 2020, the fellow attended the Society of Mathematical Biology virtual Annual Meeting (eSMB2020) and gave the contributed talk entitled “Spatial self-organization promotes coexistence between two species in nonlocal competition models.” An amount of R\$133,70 from “Reserva Técnica” was spent for registration in the event.

## 5 Publications

In this period we published the work entitled “Enhanced species coexistence in Lotka-Volterra competition models due to nonlocal interactions” on the Journal of Theoretical Biology ([Maciel and Martinez-Garcia, 2021](#)). This study was carried in the first year of the project and it was described in the previous report.

## References

- Cabal, C., Martínez-García, R., de Castro Aguilar, A., Valladares, F., and Pacala, S. W. (2020). The exploitative segregation of plant roots. *Science*, 370(6521):1197–1199.
- Dohn, J., adn Moussa Karembé, F. D., Moustakas, A., Amévor, K. A., and Hanan, N. P. (2013). Tree effects on grass growth in savannas: competition, facilitation and the stress-gradient hypothesis. *Journal of Ecology*, 101:202–209.
- Hastings, A., , Byers, J. E., Crooks, J. A., Cuddington, K., Jones, C. G., Lambrinos, J. G., Talley, T. S., and Wilson, W. G. (2007). Ecosystem engineering in space and time. *Ecology Letters*, 10:153–164.
- Hauggaard-Nielsen, H. and Jensen, E. S. (2005). Facilitative root interactions in intercrops. *Plant and Soil*, 274:237–250.
- Ludwig, F., Dawson, T. E., Prins, H. H. T., Berendse, F., and de Kroon, H. (2004). Below-ground competition between trees and grasses may overwhelm the facilitative effects of hydraulic lift. *Ecology Letters*, 7:623–631.
- Maciel, G. A. and Martinez-Garcia, R. (2021). Enhanced species coexistence in lotka-volterra competition models due to nonlocal interactions. *Journal of Theoretical Biology*, 530:110872.



# Enhanced species coexistence in Lotka-Volterra competition models due to nonlocal interactions



Gabriel Andreguetto Maciel, Ricardo Martinez-Garcia<sup>\*</sup>

ICTP South American Institute for Fundamental Research & Instituto de Física Teórica, Universidade Estadual Paulista - UNESP, Rua Dr. Bento Teobaldo Ferraz 271, Bloco 2 - Barra Funda, 01140-070 São Paulo, SP, Brazil

## ARTICLE INFO

### Article history:

Received 10 December 2020

Revised 13 July 2021

Accepted 15 August 2021

Available online 20 August 2021

### Keywords:

Pattern formation

Integro-differential models

Lotka-Volterra systems

Ecological communities

## ABSTRACT

We introduce and analyze a spatial Lotka-Volterra competition model with local and nonlocal interactions. We study two alternative classes of nonlocal competition that differ in how each species' characteristics determine the range of the nonlocal interactions. In both cases, nonlocal interactions can create spatial patterns of population densities in which highly populated clumps alternate with unpopulated regions. These non-populated regions provide spatial niches for a weaker competitor to establish in the community and persist in conditions in which local models predict competitive exclusion. Moreover, depending on the balance between local and nonlocal competition intensity, the clumps of the weaker competitor vary from M-like structures with higher densities of individuals accumulating at the edges of each clump to triangular structures with most individuals occupying their centers. These results suggest that long-range competition, through the creation of spatial patterns in population densities, might be a key driving force behind the rich diversity of species observed in natural ecological communities.

© 2021 Elsevier Ltd. All rights reserved.

## 1. Introduction

The competitive exclusion principle predicts that two species competing for the same resource cannot coexist if environmental factors are constant (Gause, 1934; Hardin, 1960). However, this contrasts with the large number of competitors that often coexist in ecological communities (Hutchinson, 1961). Unveiling this paradox and explaining how competing species coexist in nature has been a long-standing goal of ecological theory (May, 1972; Tilman, 1982; Chesson, 2000; Tokeshi, 2009). Some of the mechanisms that have been proposed to explain the coexistence of competing species rely on environmental fluctuations either in space or time (Amarasekare, 2003; Chesson, 2000; Maciel et al., 2018), diet differentiation (Kartzin et al., 2015), higher-order or frequency-dependent interactions (Grilli et al., 2017; Ayala, 1971), or trade-offs between fitness components (Levins et al., 1971; Kneitel et al., 2004; Cadotte et al., 2006; Angert et al., 2009; Tamita et al., 2015; Martínez-García et al., 2017; Martínez-García et al., 2021b).

Without any of these ingredients, classical models like Lotka-Volterra predict that two competitors only coexist if individuals

from each species compete more strongly with their relatives than with individuals from the other species (Murray, 2002; Chesson, 2000). However, the original Lotka-Volterra model assumes that the populations are well-mixed and two individuals are equally likely to interact with each other regardless of their location (Durrett and Levin, 1994; Lee et al., 2001; Hutchinson et al., 2007; O'Dwyer, 2020). This assumption requires that the interaction's spatial scale is negligible compared to the spatial scales of movement, which is not valid for several biological systems (Hutchinson et al., 2007; Holmes et al., 1994; Tilman and Kareiva, 1997; Martínez-García et al., 2020). Most often, populations are not perfectly mixed, and individuals only interact with neighbors within a small region around them (Lee et al., 2001).

Nonlocal competition (i.e., competition between a focal individual and its neighbors within a finite range) is frequent in natural systems and has been suggested to underlie the emergence of non-uniform spatial distributions of individuals. For example, Martínez-García et al., (Martínez-García et al., 2013; Martínez-García et al., 2014; Martínez-García et al., 2021a) showed that nonlocal competition alone can create regular vegetation patterns in water-limited ecosystems. In competitive communities, species arrange in regularly spaced clumps on the abstract niche space due to nonlocal competition (Scheffer and van Nes, 2006; Pigolotti et al., 2007; Fort et al., 2009). Several territorial species and central-place foragers often create a hexagonal, overdispersed

<sup>\*</sup> Corresponding author.

E-mail address: [ricardom@ictp-saifr.org](mailto:ricardom@ictp-saifr.org) (R. Martínez-García).

# Final Scientific Report

## Modern Methods for Scattering Amplitudes in Field (Gauge Theories and Gravity) and String Theory

Postdoc: Diego Medrano Jiménez

Supervisor: Nathan Berkovits

FAPESP process: [2019/07286-3](#)

Reporting period: 1/10/2019 to 31/12/2021



# Final Scientific Report

(October 1, 2019 – December 31, 2021)

Diego Medrano Jiménez - d.medrano@ictp-saifr.org  
Instituto de Física Teórica ICTP-SAIFR  
Rua Dr. Bento Teobaldo Ferraz, 271-Bloco 2  
Barra Funda, 01140-070 São Paulo, Brasil

---

## 1 Research

During the grant, my research has been focused mainly in the context of the S-matrix bootstrap and integrability. In particular, these are the topics of the FAPESP position project I have been working on:

### 1.1 Elliptic deformation (ED) of supersymmetric sine-Gordon (ssG)

The *S-matrix bootstrap* program aims at exploring and delimiting the space of 2-dimensional QFTs consistent with the presence of certain symmetries and for which the two-to-two scattering amplitudes are *analytic*, *crossing symmetric* and *unitary*. The great advantage of this approach is that it allows to study and classify theories non-perturbatively including both weak and strong couplings. Normally the most interesting ones are those that saturate unitarity, located at the boundary of the allowed region, because in many cases their S-matrices turn out to fulfill as well the Yang-Baxter equation. These theories are said to be *integrable*.

In particular, within the space of  $\mathbb{Z}_2$ -symmetric trilinear couplings studied in [1], an unknown theory was discovered at the boundary and characterized as an integrable continuous deformation of ssG. It does not preserve supersymmetry but comes with an interesting periodic energy behavior that can be described by Jacobi elliptic functions. The theory was called *elliptic deformation* (ED) of ssG and, although the exact S-matrix can be checked in [2], a lagrangian description is still missing. One of the objectives of this research project was to study the nature of the new interactions among the ssG fields giving rise to the deformation, and to obtain a complete lagrangian in closed form if possible.

First of all, we decided to use perturbation theory and compute the Taylor expansion of the exact S-matrix in the deformation parameter  $\kappa$ . This would allow for a direct connection between the theory and its tree-level amplitudes. However, the integral representation of its phase makes it non-trivial to perform. The final expansion can be obtained by exploiting the periodicity of the integrand and splitting the whole expression into different patches. As a result, we managed to write all the two-to-two scattering amplitudes of the theory up to third order in  $\kappa$ . The idea was to read directly the new couplings of the deformation and to guess the corresponding vertices through the rapidity  $\theta$  dependence, which can be perfectly reproduced just by including derivative contractions among the fields. Loop order computations can also be used as a crosscheck for the new obtained interactions. Nevertheless, the procedure is quite ambiguous since many of these vertices give the same contribution to the amplitude. Therefore a new strategy was needed, which follows from exploiting one of the main features of the theory: *integrability*.

## 1.2 Integrable deformations of sG and ssG: no-particle production

A theory is said to be integrable whenever its  $n$ -point S-matrix can be factorized into a product of two-to-two processes and those smaller matrices fulfill the Yang-Baxter equation. A direct consequence is that these theories present *no-particle production* at all orders. Therefore, imposing no-particle production from scratch in the presence of some particular matter content, constitutes a powerful tool for finding integrable theories and identifying their local interactions to build a lagrangian. Examples of the identification of pure bosonic as well as some supersymmetric extensions can be found in [3,4] respectively.

This method should also be useful in the context of  $T\bar{T}$  theories. In general,  $T\bar{T}$  is an integrable irrelevant deformation that can be computed for any theory from its stress-energy tensor  $T_{\mu\nu}$  [5,6], that shifts every element of the S-matrix by a constant phase —i.e. CDD-factors—. It belongs to a broader family of integrable deformations known as  $X_s$  deformations [7], for which a lagrangian description is also still missing.

In order to get familiar with no-particle production in our set-up, we decided to start with the pure bosonic case and try to identify integrable deformations of sine-Gordon (sG) just by including derivative interactions in the theory. We started constructing independent 4- and 6-point bosonic vertices with different derivative contractions —i.e. independent Mandelstam  $s_{ij}$  polynomials— and imposing tree-level two-to-four amplitudes to vanish —i.e. imposing  $M_{2\rightarrow 4} = 0$ —. As expected, we were able to write an effective lagrangian for the  $T\bar{T}$  deformation of sG, which is in agreement with the closed form found in [8]; and additionally, we found a different solution and wrote an effective lagrangian consistent with the leading behavior of the  $X_3$  deformation of sG at tree-level. Subleading terms in these effective lagrangians would come by imposing  $M_{2\rightarrow 6} = \dots = M_{2\rightarrow n} = 0$ , however this becomes computationally more and more expensive very fast.

Proceeding in an analogous way now with fermions in supersymmetric sine-Gordon (ssG), we started looking at all possible Lorentz invariant structures (vertices including derivatives) out of the field content of the undeformed theory ssG, and constructing the corresponding tree-level amplitudes to impose no-particle production at leading order. Again, we managed to write an effective lagrangian for  $T\bar{T}$ -ssG, matching the correct behavior of the S-matrix at leading order, and in agreement with the general lagrangian obtained from the flow equations presented in [8]. In this case, we also found various different solutions, some of them compatible with ED-ssG, which would correspond to new unknown deformations of ssG. In order to completely identify ED-ssG, we should keep imposing no-particle production at next-leading-orders —i.e. vanishing higher-point amplitudes—, reducing at the same time the number of solutions; however, this can be challenging since we do not have yet an optimized algorithm to include all new possible  $n$ -point derivative interactions in a systematic way. This part is ongoing work.

In summary, we obtained expressions for the effective lagrangians of various bosonic — $T\bar{T}$ -sG and  $X_3$ -sG— and fermionic — $T\bar{T}$ -ssG and ED-ssG— deformations. Ideally, once we have improved our computations for imposing no-particle production at higher-point amplitudes, we would be closer to start guessing the exact lagrangians beyond perturbation theory —i.e. resummed to all orders.

## 1.3 Integrable deformations of sG and ssG: Lax pairs

In the case of  $T\bar{T}$ , the closed form of the lagrangian can be obtained directly by solving the corresponding flow equation of the deformation [8]. We computed both  $T\bar{T}$ -sG and  $T\bar{T}$ -ssG, and compared them with the results from no-particle production finding perfect agreement.

In order to obtain the exact lagrangians of  $X_3$ -sG and ED-ssG, until we optimize our computations in no-particle production, we are exploring integrability from a different point of view: the existence of a *Lax pair* [9]. Starting from the Lax pair of sG and ssG, the idea is to find all possible deformations that keep the flatness condition invariant [10]. During the last months, we have become quite familiar with the bosonic case and started playing around to find the  $X_3$ -sG Lax pair. General deformations of the ssG Lax pair have still to be done. Once we finish, this would allow us to write directly the equations of motion of both deformed theories and from there try to guess the exact expressions for the lagrangians. Computations on this section are mainly future work.

## 2 Publications

The results derived from these topics are expected to lead to two different publications:

The first one will collect results from the bosonic computations mentioned above. It will be presented the effective lagrangian of the  $X_3$ -sG theory obtained from no-particle production and, once its Lax pair is studied in detail, it will serve to delve into the general structure of the  $X_n$  integrable deformations. The idea is to find as well the  $X_3$ -sG lagrangian in closed form once the no-particle production algorithms are automatized.

The second one will present the effective lagrangian found for ED-ssG and will serve to study in detail its integrability structure through the existence of a Lax pair. Again, a lagrangian in closed form —written presumably in terms of Jacobi elliptic functions— will be presented if possible once the no-particle production computations are improved.

## 3 Seminars and conferences

- Simons Collaboration on the Nonperturbative Bootstrap Annual Meeting 2019. November 7-8, 2019. (New York - USA)
- Zoomplitudes 2020. May 11-15, 2020.
- Bootstrap 2020. June 1-26, 2020.
- Bootstrap School 2020. June 8-12, 2020.
- Strings 2020. June 29 - July 3, 2020.
- Snowmass Theory Frontier meeting. July 30, 2020.
- Integrability in Gauge and String Theory IGST 2020. August 24-28, 2020.
- Positivity and the Bootstrap. May 31 - June 2, 2021.
- Strings 2021. June 21 - July 2, 2021.
- Bootstrap School 2021. July 5-23, 2021.
- Bootstrap Workshop 2021. July 5-23, 2021.
- Amplitudes 2021. August 16-20, 2021.

## 4 Activities

I have been organizing the weekly String Theory Journal Club, inviting different speakers to give specialized talks at the ‘Instituto de Física Teórica IFT-UNESP’.

## References

- [1] A. Homrich, J. a. Penedones, J. Toledo, B. C. van Rees and P. Vieira, *The S-matrix Bootstrap IV: Multiple Amplitudes*, [JHEP 11 \(2019\) 076](#) [1905.06905](#).
- [2] C. Bercini, M. Fabri, A. Homrich and P. Vieira, *SUSY S-matrix Bootstrap and Friends*, [1909.06453](#).
- [3] B. Gabai, D. Mazáč, A. Shieber, P. Vieira and Y. Zhou, *No Particle Production in Two Dimensions: Recursion Relations and Multi-Regge Limit*, [JHEP 02 \(2019\) 094](#) [1803.03578](#).
- [4] C. Bercini and D. Trancanelli, *Supersymmetric integrable theories without particle production*, [Phys. Rev. D 97 \(2018\) 105013](#) [1803.03612](#).
- [5] A. B. Zamolodchikov, *Expectation value of composite field  $T$  anti- $T$  in two-dimensional quantum field theory*, [hep-th/0401146](#).
- [6] A. Cavaglià, S. Negro, I. M. Szécsényi and R. Tateo,  *$T\bar{T}$ -deformed 2D Quantum Field Theories*, [JHEP 10 \(2016\) 112](#) [1608.05534](#).
- [7] F. Smirnov and A. Zamolodchikov, *On space of integrable quantum field theories*, [Nucl. Phys. B 915 \(2017\) 363](#) [1608.05499](#).
- [8] G. Bonelli, N. Doroud and M. Zhu,  *$T\bar{T}$ -deformations in closed form*, [JHEP 06 \(2018\) 149](#) [1804.10967](#).
- [9] A. Torrielli, *Lectures on Classical Integrability*, [J. Phys. A 49 \(2016\) 323001](#) [1606.02946](#).
- [10] R. Conti, L. Iannella, S. Negro and R. Tateo, *Generalised Born-Infeld models, Lax operators and the  $T\bar{T}$  perturbation*, [JHEP 11 \(2018\) 007](#) [1806.11515](#).

---

---

## Scientific Report 2021

---

---

Title	Correlations in many-body systems from the perspective of DFT, QIT and RG
Postoc	Krissia de Zawadzki
Supervisor	Nathan Jacob Berkovits
Fapesp process	2020/13115-4
Period	01/Dec/2020- 31/Oct/2021

Nathan Berkovits



INTERNATIONAL CENTER FOR THEORETICAL PHYSICS  
SOUTH AMERICAN INSTITUTE FOR FUNDAMENTAL RESEARCH

## Abstract

In this report, we provide an overview of the projects and activities developed by Krissia de Zawadzki at ICTP-SAIFR from December 2020 to September 2021. The ultimate goal of her research proposal is to understand strongly correlated systems in and out-of-equilibrium and design methods to calculate their properties accurately. To this aim, it is proposed to combine tools from condensed matter physics well established for many-body systems, namely, Renormalization-Group (RG) and Density Functional Theory (DFT) with concepts of Quantum Information Theory (QIT), mainly entanglement. Here, results of three projects applying the latter idea are presented. The first one investigates density functional approximations to describe the extracted quantum work and the entropy production across the Mott-insulating and superfluid transitions. In the second project, we analyze the effects of the temperature in the entanglement and linear entropy across Mott metal-insulator transition (MIT) triggered by disorder or by Coulomb interaction. Finally, the third project discusses an interferometric protocol to perform quantum thermometry in a correlated electronic system. Academic activities in which the researcher got involved are also presented.

# 1 Research

## 1.1 Density Functional approximations for Quantum Thermodynamics

Quantum Thermodynamics has become one of the most interesting research fields in the past decades. It emerged from the need to re-define quantities such as work, heat and entropy at the quantum scales, for which the thermodynamic limit does not hold as in traditional statistical mechanics. Understanding thermodynamical quantities in quantum systems is essential to advance quantum technologies, with applications such as quantum heat engines and quantum batteries [1–5]. For instance, the average quantum work extracted is recognized a key quantity to optimize energy consumption, whilst the thermodynamic entropy (or irreversible work) is indicative of the energy dissipated in a cycle or to reset a system to thermal equilibrium.

In Ref. [6], we have shown that to design reliable approximations for the quantum work one has to account for two main ingredients: first, the description of the initial thermal state, and, second, the evolution Hamiltonian used to emulate the dynamics. We have demonstrated that the initial thermal state is the main ingredient to build an accurate approximation, in such a way that if one can approximate the initial state as close as possible to the exact one, it is possible to improve dramatically the results for work extraction. Importantly, we show that this result holds in various thermal regimes even in the case one considers a fully non-interacting Hamiltonian to describe the unitary evolution. To push forward the accuracy of this approximation protocol, we proceeded by trying to improve the evolution operator. As in the problem of the Hubbard dimer, we resorted to a DFT approach using the Kohn-Sham (KS) Hamiltonian to describe the unitary. Focusing our attention on driven Hubbard chains with up to 8 sites, we compared to two density functional forms for the exchange-correlation potential entering the KS Hamiltonian: (i) the analytical parametrization for the ground-state energy of the Hubbard Hamiltonian extracted from its exact solution via Bethe Ansatz (BALDA) [7] and (ii) a numerical exact reverse-engineered potential calculated using the inversion scheme devised by Coe et al in [8], which we refer as GSKS. Our results indicated that these two forms improved considerably the results for approximated extracted work and entropy, especially in intermediate coupling regimes.

We consider work protocols in which the system is initially in equilibrium with a bath and its found in a thermal state  $\hat{\rho}_0 = e^{-\beta \hat{H}_0} / Z_0$ , where  $\hat{H}_0$  is the initial Hamiltonian,  $\beta = 1/k_B T$  and  $Z_0 = \text{Tr} [e^{-\beta \hat{H}_0}]$  is the partition function. This initial states then evolves from  $t = 0$  to  $t = \tau$  to an out-of-equilibrium state  $\hat{\rho}_\tau$ . The work that can be extracted during this dynamics is calculated as

$$\langle W \rangle = \text{Tr} [\hat{\rho}_\tau \hat{H}_\tau] - \text{Tr} [\hat{\rho}_0 \hat{H}_0]. \quad (1)$$

As mentioned, in order to shed light on the contributions to work extraction due to interaction effects, we first investigated how a purely non-interacting dynamics is able to reproduce the exact work extracted from a correlated Mott-insulator described by the 1D Hubbard Hamiltonian [6]. We then, investigated how approximations to quantum thermodynamics based on Density Functional Theory can improve these previous results. We propose to approximate the extracted quantum work  $\langle W \rangle$  as follows

$$\langle W^{is+evo} \rangle = \text{Tr} [\rho_f^{is+evo} \hat{H}^{evo}(t = \tau)] - \text{Tr} [\rho_0^{is} \hat{H}^{evo}(t = 0)], \quad (2)$$

where *is* (initial system) refers to the approximation used to derive the initial state,  $\rho_0^{is} = \exp(-\beta \hat{H}^{is}(0)) / \text{Tr} [\exp(-\beta \hat{H}^{is}(0))]$ , and *evo* is the approximation used for the evolution operator  $\mathcal{U}_{evo} = \mathcal{T} e^{-i \int_0^\tau \hat{H}^{evo}(t) dt}$  where  $\mathcal{T}$  is the time-ordered operator. The final state is then  $\rho_f^{is+evo} = \mathcal{U}_{evo} \rho_0^{is} \mathcal{U}_{evo}^\dagger$ . In the ‘simple’ approximations, as *is* and *evo* are the same, meaning that the evolution Hamiltonian and the initial state are both approximated according to the choice for the exchange-correlation functional. In the ‘hybrid’ approximations, the initial state is the exact thermal state, so that even though the evolution operator represents a poor approximation for the dynamics, the initial populations of the many-body eigenstates at  $t = 0$  are accurate. Under the assumption that  $\rho_0$  can be calculated with good accuracy using any approximation method, it has been demonstrated that it is possible to obtain results with reasonable accuracy in a great part of the parameter space  $U$  vs  $\tau$  [6].

We also studied approximations for entropy production, which is directly associated with irreversibility. Approximations for entropy are calculated as [6]

$$\Delta \Sigma = \beta (\langle W^{is+evo} \rangle - \Delta F^{is}). \quad (3)$$

We apply the latter DFT-inspired approximation to investigate the work extraction in a driven strongly correlated electronic system described by the Hubbard model in 1D. The corresponding Hamiltonian reads:

$$\hat{H}(t) = -J \sum_{i,\sigma}^N \left( \hat{c}_{i,\sigma}^\dagger \hat{c}_{i+1,\sigma} + \hat{c}_{i+1,\sigma}^\dagger \hat{c}_{i,\sigma} \right) + U \sum_i^N \hat{n}_{i,\uparrow} \hat{n}_{i,\downarrow} + \sum_i^N v_i(t) \hat{n}_i, \quad (4)$$

where  $N$  is the number of sites,  $J$  is the hopping term,  $U$  is the Coulomb interaction strength on site  $i$ , and  $v_i(t)$  is the time-dependent driving potential at site  $i$ . The creation (annihilation) operator for a fermion with spin  $\sigma$  ( $\sigma = \uparrow$  or  $\downarrow$ ) at site  $i$  is  $\hat{c}_{i,\sigma}^\dagger$  ( $\hat{c}_{i,\sigma}$ ), and its number operator is  $\hat{n}_i = \hat{n}_{i,\uparrow} + \hat{n}_{i,\downarrow}$ , where  $\hat{n}_{i,\sigma} = \hat{c}_{i,\sigma}^\dagger \hat{c}_{i,\sigma}$ . The number of particles  $n_\uparrow$  and  $n_\downarrow$  determines the subspace in which the matrix Hamiltonian  $H$  can be diagonalized. The external driving  $v_i(t)$  is turned on between  $t = 0$  and  $t = \tau$ . In the present, we considered drivings of the form  $v_i(t) = \mu_i^0 + \mu_i^\tau t / \tau$ , so that  $\tau$  controls the velocity of the driving.

Our analysis is carried out with a six site chain at half filling in the subspace  $S_z = 0$ . We set  $\mu_i^0 = 0.5J$  and  $\mu_i^\tau = 4.5J$ , so that most effects associated with a Mott-insulating state

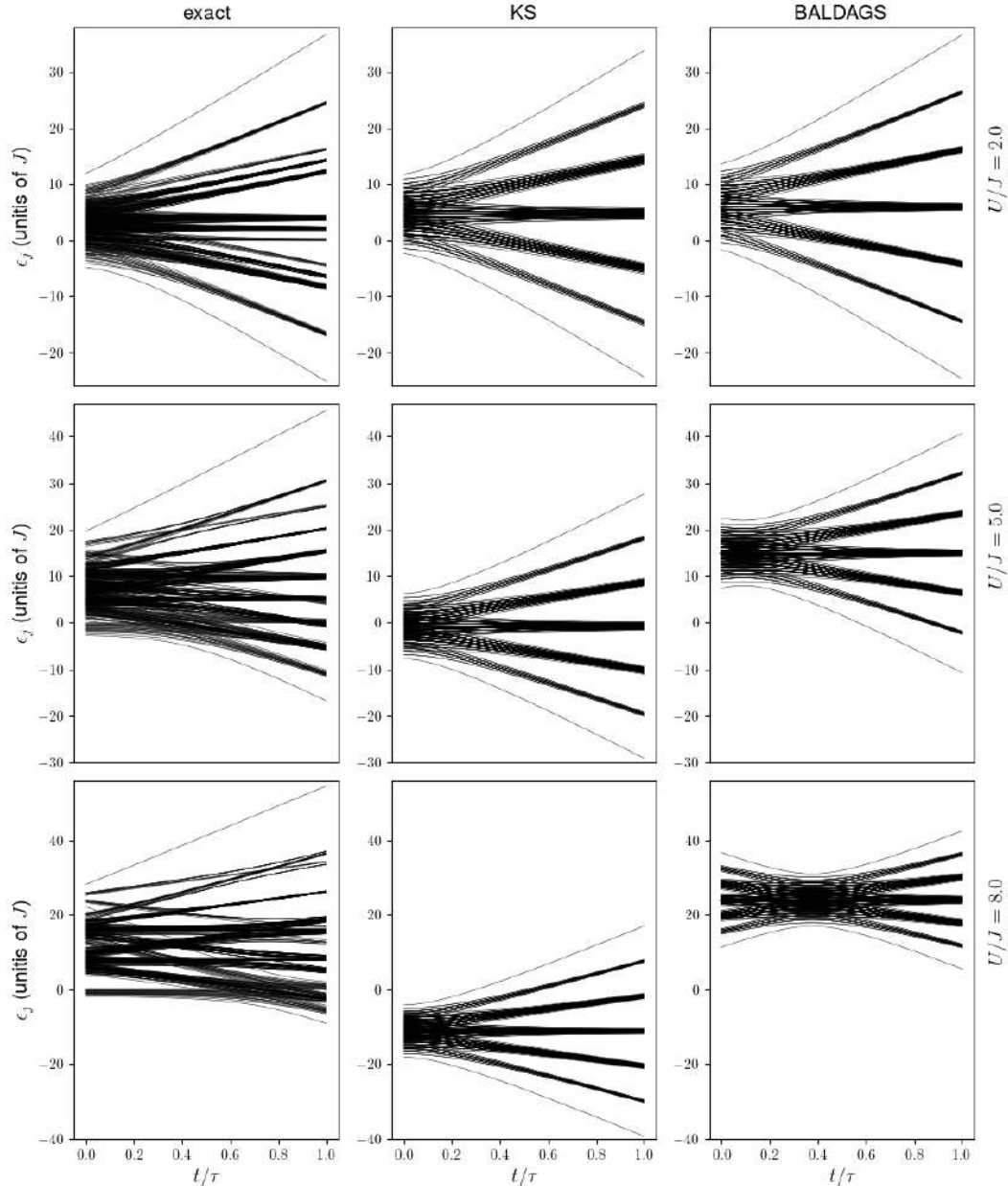


Figure 1: Upper panels: exact (left), simple GSKS (centre), and simple BALDA (right) instantaneous spectra for  $U = 2J$ . Central and lower panels: as for upper panels, but for  $U = 5J$  and for  $U = 8J$ , respectively. Here the low-temperature simple-BALDA is used, but difference with higher temperatures are minimal.

should depict close to  $U \geq 5J$ . The main findings of our work are summarized in Figs 1, 2, 3 and 4, where we show, respectively, the exact versus the approximated spectra, the normalized accuracy of the BALDA and the GSKS approximations, and a diagram showing which approximation is better in each interaction and dynamical regimes. Overall, the BALDA and the GSKS approximations improve considerably the approximations for the extracted work compared to the non-interacting approximation studied in Ref. [6], especially at intermediate coupling regimes of  $2 \leq U \leq 6$ . This result can be interpreted with the aid of the approximated spectra in Fig. 1: while qualitatively, the driven allows to reproduce the exact spectra at all times for  $U \approx 2J$ , as the Coulomb repulsion increases, many-body features are lost and

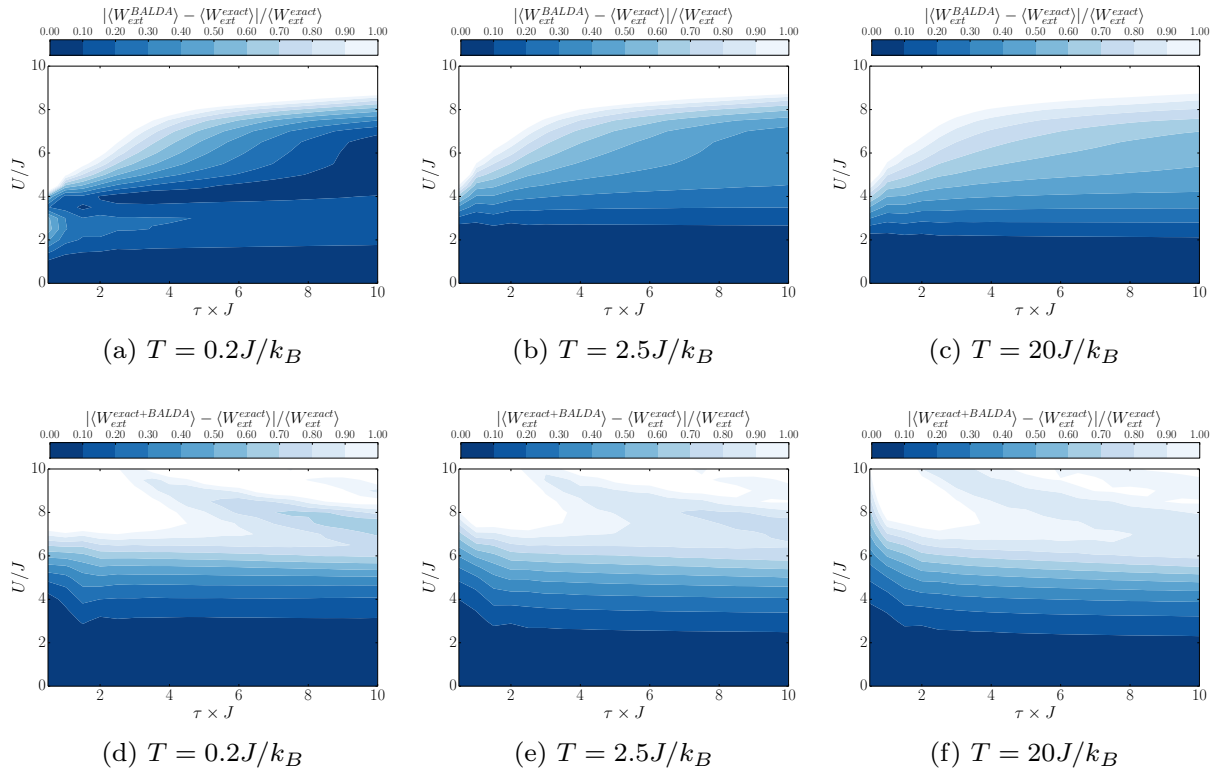


Figure 2: Relative difference between the simple and hybrid BALDA approximations for the extracted work . Darker blue tones correspond to higher accuracy).

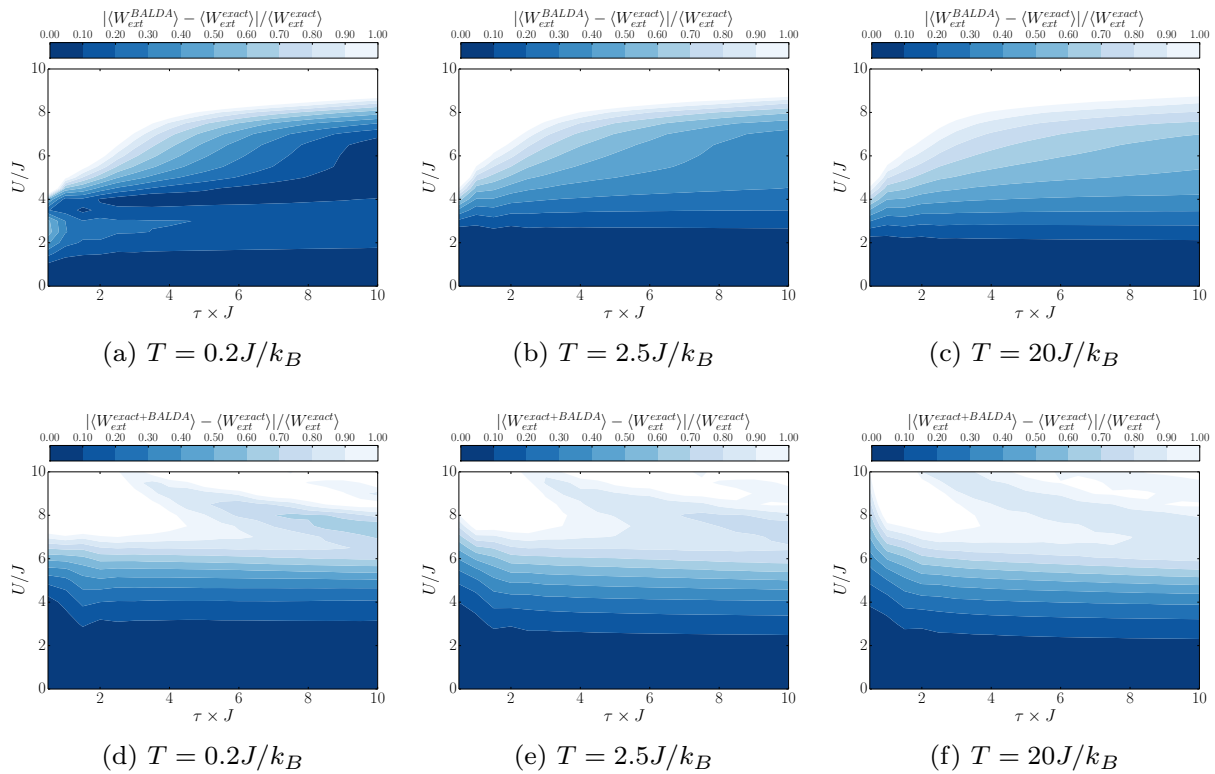


Figure 3: Relative difference between the simple and hybrid GSKS approximations for the extracted work . Darker blue tones correspond to higher accuracy).

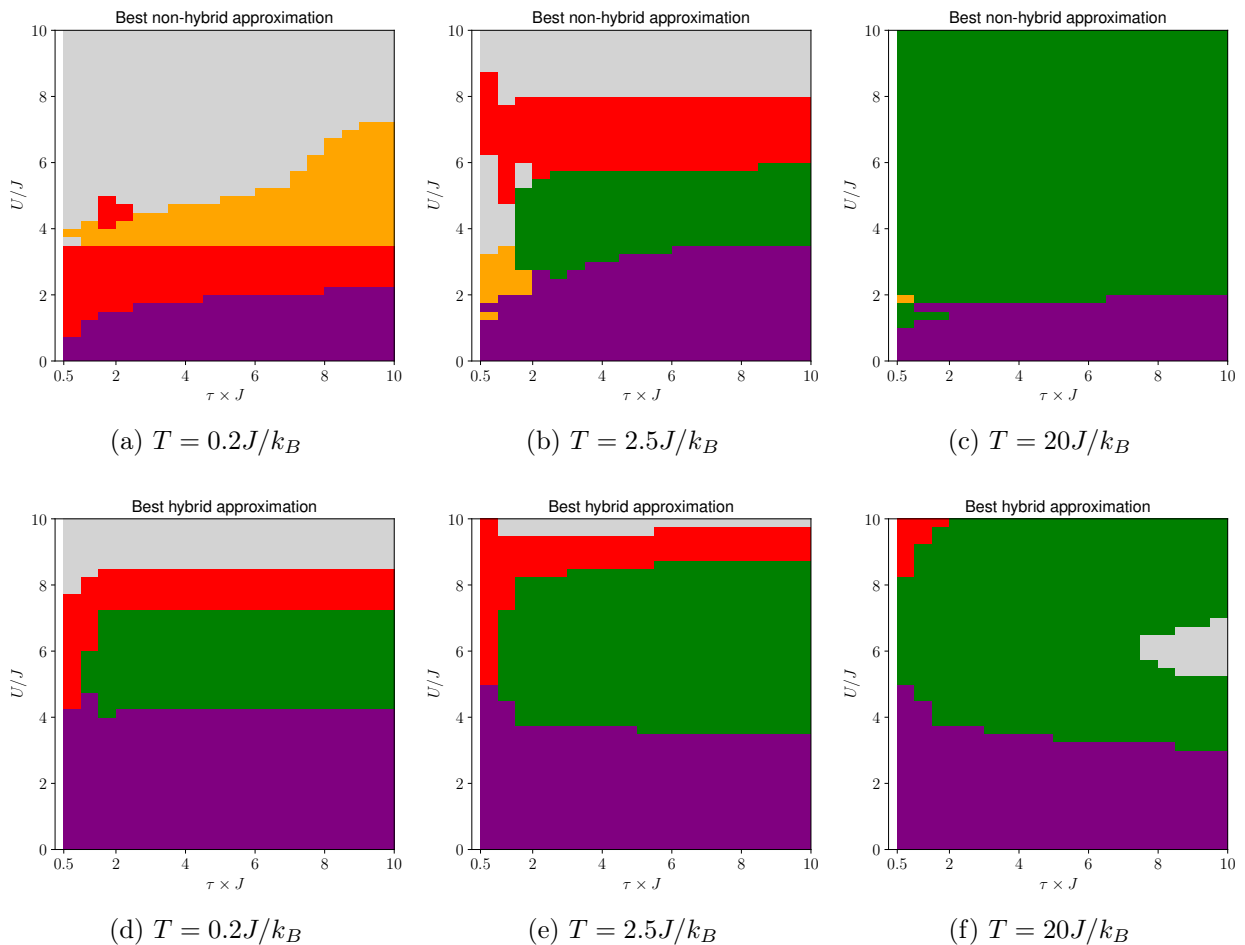


Figure 4: Upper panels: Figures showing which ‘simple’ approximation is most accurate (up to 20%) for the work extraction. The colours representing the approximations are **all**, **non-interacting**, **BALDA**, and **GSKS**. Lower panels: Figures showing which hybrid approximation is most accurate (up to 20%) for the entropy production. The colours representing the approximations are **all**, **‘exact + NI’**, **‘exact + BALDA’**, and **‘exact + GSKS’**, seen here.

the dynamics can no longer describe the interacting system accurately. Additionally, from low to high temperatures, hybrid approximations in the bottom panels of Figs. 2 and 3, in which the initial state is the exact one, depict better agreement in comparison to the simple protocol shown in the top panels. By inspecting Fig. 3, we observe that it is possible to reproduce the extracted work with accuracy up to 20% by means of the hybrid approach which uses the GSKS potential to approximate the evolution operator describing the dynamics of the system. The same error criteria applied to the entropy reveals that this quantity requires extra ingredients to build accurate approximations, especially at low temperatures. Nonetheless, in most of the parameter space and for all temperatures studied, the performance of such approximation is comparable to a protocol that neglects interactions completely, as that explored in Ref. [6]. At low temperatures, specially when  $U \approx v_i$ , errors are above 20%.

In Fig. 4, we show which simple or hybrid approximation are most accurate to reproduce the work with up to 20% of error. Note that for  $U \leq 4J$ , all hybrid approximations provide reasonable accuracy. Once the non-interacting evolution is cheaper compared BALDA and GSKS, one could easily obtain accurate results without approximating the evolution operator

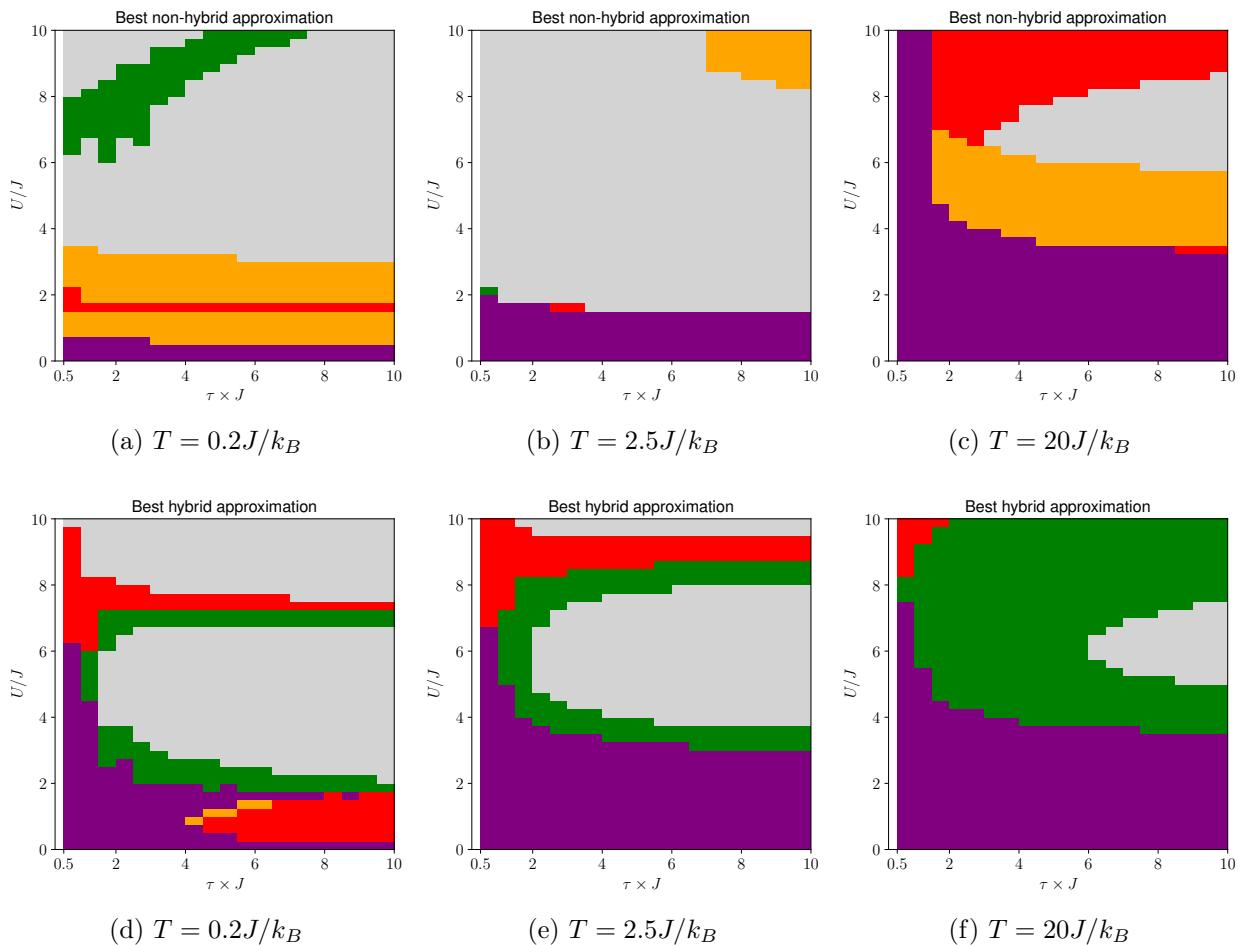


Figure 5: Same of Fig. 4 for the entropy.

with a DFT-inspired calculation or more expensive methods.

A comparison between simple and hybrid approximations for the entropy is shown in Fig. 5.

We show that for ‘hybrid’ approximations (lower row of figure ??) the relative error on the entropy variation is related to the corresponding error on the extracted work as follows

$$\frac{|\Delta\Sigma_{exact} - \Delta\Sigma_{approx}|}{|\Delta\Sigma_{exact}|} = R_{exact} \frac{|\langle W_{ext}^{exact} \rangle - \langle W_{ext}^{approx} \rangle|}{|\langle W_{ext}^{exact} \rangle|}, \quad (5)$$

with

$$R_{exact} = \frac{1}{k_B T} \frac{|\langle W_{ext}^{exact} \rangle|}{|\Delta\Sigma_{exact}|}. \quad (6)$$

This indicates that only where  $R_{exact} \leq 1$  the hybrid approximation for the entropy variation is at least as good as the corresponding one for the average work. Note that as  $\Delta F$  is exact, an improvement over the approximation of  $\langle W_{ext} \rangle$  should directly reflect on the quality of the approximation for  $\Delta\Sigma$ . Interestingly, the hybrid GSKS approximation for  $\Delta\Sigma$  overperforms all the others especially in the sudden quench and strong interaction regimes.

These important results provide a reasonable framework to study work extraction in out-of-equilibrium correlated systems, much cheaper than more complicated approximations.

## 1.2 Entanglement entropy at criticality and temperature effects

Entanglement has been proposed as a witness of quantum phase transitions [9, 10] in many body systems depicting strong correlations. In the particular case of systems described by Hubbard-like Hamiltonians in 1D, one can explore a plethora of phases ranging from metal, insulator and superfluid [11, 12].

The metal-to-insulator transition (MIT), it has been shown that the *single-site entanglement* can be used as a witness, as its discontinuity occurs at critical points [13]. In the absence of interactions, such mechanism can be triggered by coherent backscattering from randomly distributed impurities and leads to a phase known as Anderson-MIT. On the other hand, in the presence of a strong Coulomb repulsion, i.e. electron-electron interactions, the Mott physics comes into play. In both regimes, the entanglement depicts a minimum at critical densities, and become more pronounced as the impurity potential increases  $|V| \ll U$ . A superfluid phase [14] can also emerge by means of an attractive Coulomb repulsion and due to the presence of impurities randomly distributed along the Hubbard chain. At critical concentrations of impurities, the ground-state is fully-localized and the entanglement vanishes. The competition between the electron-electron interaction and disorder leads to a non-trivial ground-state whose entanglement is characterized by a richer behavior, with a set of local minima revealing new phases of partial localization.

Following previous works by Canella and França, we investigated the effects of concentration, magnetization and temperature on the entanglement across the Mott-Anderson transition and, further extended the analysis of the superfluid-Mott transition to the realm of Quantum Thermodynamics.

The systems we investigate are described by the Hamiltonian

$$\hat{H} = -J \sum_{i,\sigma}^L \left( \hat{c}_{i,\sigma}^\dagger \hat{c}_{i+1,\sigma} + \hat{c}_{i+1,\sigma}^\dagger \hat{c}_{i,\sigma} \right) + U \sum_i^L \hat{n}_{i,\uparrow} \hat{n}_{i,\downarrow} + \sum_i^L V_i \hat{n}_i, \quad (7)$$

with  $c_i^\dagger(c_i)$  being creation (annihilation) fermionic operators and  $n_i$  being the number operators acting on site  $i = 1, \dots, L$ , where  $L$  is the length of the chain. The unit of energy  $J$  is the hopping parameter, while  $U$  accounts for the electron-electron interaction that can be repulsive  $U > 0$  or attractive  $U < 0$ . The latter case allows us to explore the superfluid phase.  $V_i$  represents the external potential of the randomly distributed impurities, whose concentration is  $C_V = N_V/L$ ,  $N_V$  being the number of impurities. The impurity potential can also be attractive or repulsive.

We briefly explore our main findings in the following subsections.

### 1.2.1 Entanglement across the Mott-Anderson transition: the hole of the temperature and magnetization

The single-site entanglement is defined from the bipartite entanglement between a site labeled by  $i$  with all remaining sites  $j \neq i$  of the chain. For a pure state  $|\Psi\rangle$ , is calculated by means of the one-body reduced density matrix

$$\rho_i = \text{Tr}_{j \neq i} |\Psi\rangle \langle \Psi|. \quad (8)$$

The diagonal version of  $\rho_i$  defined above is expressed in terms of the probability finding site  $i$  double occupied  $w_{2,i} = \langle \Psi | \hat{d}_i | \Psi \rangle$ , where  $\hat{d}_i = \hat{c}_{\uparrow,i}^\dagger \hat{c}_{\downarrow,i}^\dagger$  defines the doublon operator, singly occupied with a spin up  $w_{\uparrow,i} = \langle \Psi | \hat{n}_{\uparrow,i} | \Psi \rangle - w_{2,i}$  or down  $w_{\downarrow,i} = \langle \Psi | \hat{n}_{\downarrow,i} | \Psi \rangle - w_{2,i}$ , or and

empty empty  $w_{0,i} = 1 - w_{2,i} - w_{\uparrow,i} - w_{\downarrow,i}$ . It reads

$$\rho_i = \begin{pmatrix} w_{0,i} & 0 & 0 & 0 \\ 0 & w_{\uparrow,i} & 0 & 0 \\ 0 & 0 & w_{\downarrow,i} & 0 \\ 0 & 0 & 0 & w_{2,i} \end{pmatrix}. \quad (9)$$

The definition above also holds at finite temperature, where now, the local operators  $\mathcal{O} = n_{i\sigma}, d_i$  are calculated as

$$\langle \mathcal{O} \rangle = \text{Tr}\{\hat{\mathcal{O}}\hat{\rho}_\beta\}, \quad (10)$$

where  $\hat{\rho}_\beta$  is a thermal state at inverse temperature  $\beta = 1/k_B T$ .

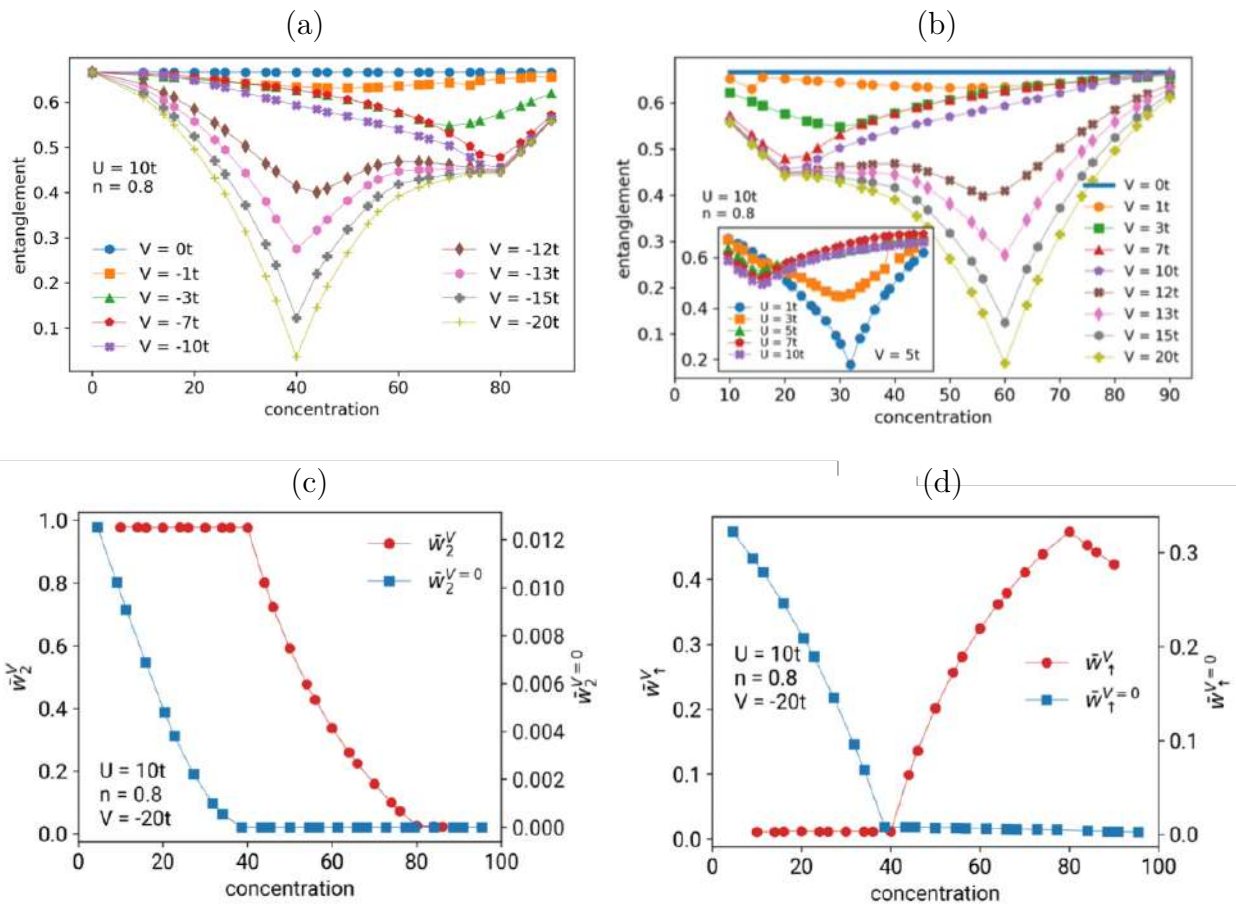


Figure 6: Average single-site entanglement as a function of the concentration of impurities for various strengths  $V$  at fixed  $U = 10J$ . (a) and (b) show  $\langle S_i \rangle$  for repulsive and attractive  $V$ , respectively. (c) and (d) show the probabilities of double  $w_2^V$  and singly  $w_\uparrow$  occupation at impurity  $w_\sigma^V$  and non-impurity  $w_\sigma^{V=0}$  sites.

We focus our analysis in the average single-site entanglement  $\langle S_i \rangle$  as a function of the concentration of impurities. At zero temperature, i.e., ground-state, results can be obtained for large systems of  $L = 100$  sites using numerical methods such as the Density Matrix Renormalization-Group (DMRG) method or an approximation based in Density Functional Theory (DFT), as described in [14]. At finite temperature, our results are calculated via

Exact Diagonalization (ED) of systems with  $L = 8$  sites. The latter calculation comprises a Hilbert space with around five thousand states.

In the ground-state, Mott-Anderson physics is governed by the interplay between  $U$  and  $V$ . In Fig. 6 panels (a) and (b), we show the average single-site entanglement as a function of the concentration of impurities for a system with density  $n = 0.8$  and  $L = 100$  sites, and various impurity strengths  $V$ . The attractive  $V < 0$  and repulsive  $V > 0$  cases are particle-hole symmetric. Full Anderson localization depicts in the limit when  $\langle S_i \rangle \rightarrow 0$ . In fact, the system hosts this state at critical concentrations  $C_C = 100n/2$  for  $V < 0$  and  $C_C = (1 - n/2)100$  for  $V > 0$  whenever the impurity strength is larger than the Coulomb repulsion. A local minimum is also observed at  $C_C^* = 100n$  for  $V < 0$  and  $C_C^* = (1 - n)100$  for  $V > 0$ , and it is associated with the Mott-like localization, in which the effective density is as the entire chain is at half filling. To contemplate this behavior, we inspect in panels (c) and (d) the probability of double  $w_2$  and single  $w_1$  occupancy along sites hosting (red) or not (blue) an impurity for attractive disorder. A large  $U$  value prevents impurity sites to be double occupied, i.e.,  $w_2 \rightarrow 0$ , while single occupation becomes maximum after the critical concentrations  $C_C$ .

We further complete our analysis by showing the effects of the magnetization and the temperature. In Fig 7 we analyze the impact of the magnetization  $m = n_\uparrow - n_\downarrow$  on the entanglement minimum related to the full Anderson localization. We find that the minimum at  $C_C$  is now split into two minima: one at  $C_{C\uparrow} = 100n_\uparrow$  and  $C_{C\downarrow} = 100n_\downarrow$ . Our results thus reveal that the full localization occurs separately for each spin species, thus with two critical densities.

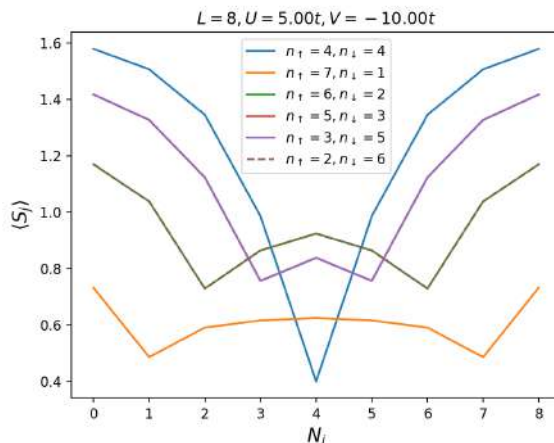


Figure 7: Dependence of the average single-site entanglement with the density for magnetized systems.

Fig. 8 shows results for  $\langle S_i \rangle$  varying with the concentration and with the temperature. Note that the blue lines in panel (a) depict essentially the same behavior of Fig. 6 observed in panel (a) for  $V = -2U$  (yellow curve). As  $T \rightarrow 0$ , the Mott-Anderson transition manifests as a minimum in the entanglement at a critical concentration  $C_C = 100n/2$ . On the other hand, increasing the temperature implies in the melting of the localized state, with a consequent increasing in the entanglement.

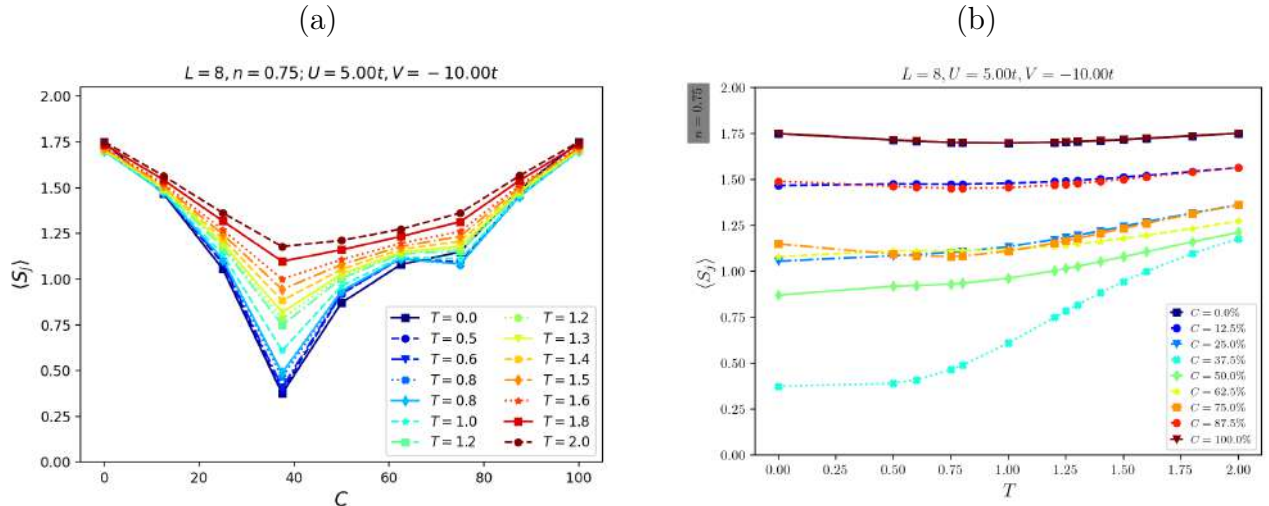


Figure 8: Dependence of the average single-site entanglement with the temperature  $T$  for various impurity concentrations.  $U = 5J$  and  $V = -10J$  are fixed. (a) shows  $\langle S_i \rangle$  as a function of the concentration for  $T \leq 2$ .

### 1.2.2 Statistics of quantum work across the superfluid-insulator transition

As discussed in sec. 1.1, the quantum work has crucial importance to design applications in Quantum Thermodynamics. For critical systems, it has been shown that the work probability distribution  $P_W$  and its statistics are very sensitive to a quench in the critical parameter [15?]. The probability distribution of work  $P(W)$  in a protocol that starts at  $t = 0$  with a Hamiltonian  $\hat{H}_0$  and finishes at  $t = \tau$  with Hamiltonian  $H_\tau$  is defined as

$$P(W) = \sum_{n,m} \delta[W - (\epsilon_m - \epsilon_n)] p_n p_{m|n}, \quad (11)$$

where  $p_n$  are the initial populations of each eigenstate  $|n\rangle$  of  $H_0$ ,  $p_{m|n}$  is the conditional probability of finding the system in the state  $|m\rangle$  of  $H_\tau$  provided it started from the initial state  $|n\rangle$ . The first moment of the work distribution gives the average ( $k = 1$ ), the second gives the variance ( $k = 2$ ) and the third gives the skewness ( $k = 3$ ):

$$\langle W^k \rangle = \int W^k P(W) dW. \quad (12)$$

In the context of the Hubbard model, we discussed the statistics of work in a finite-time protocol that drives currents across a 1D chain in order to surpass the Coulomb repulsion [16]. In particular, we have shown that the skewness of the distribution can be used as a witness of the transition, a feature that has been overlooked in the literature.

Here, we consider time-independent protocols in which two parameters are quenched to bring the Hamiltonian 7 from a superfluid to an insulator phase. In the first, we vary the disorder strength  $V_i$  keeping the concentration fixed, while in the second,  $V_i$  is fixed and the concentration is varied. Three temperatures are also considered: low  $\beta = 100J$ , intermediate  $\beta = 0.5J$  and high  $\beta = 1/30J$ . We focus our analysis in the superfluid phase supported by a Coulomb repulsion amounting for  $U = -5J$  and considered chains up to six sites at half-filling  $n = 1$ . All results are obtained using exact diagonalization.

Our results revealed that the optimal quench protocol to extract the maximum work is that in which the concentration is varied between the initial and final states. We present

the average, variance, and skewness of the work distribution of this protocol in are shown in Fig. 9. Inspecting panels (a), (d) and (g) work can only be extracted at low and moderate temperature regimes. If the disorder strength is kept fixed,  $V > U$  work extraction is amplified at the critical concentration  $C_C$ , the latter is the same at which the entanglement is minimal, as discussed in Sec. 1.2.1 Interestingly, at the critical concentration  $C_C$ , the distribution has no dispersion, as the variance vanishes. Similarly to the previous results for driven Hubbard chains of Ref. [16], the skewness of the distribution is very sensitive to the transition, its derivative depicts a discontinuity at  $C_C$ .

At high temperatures, however, the signatures of the transition disappears, as seen in panels (g)-(i). For both quench protocols, one can only produce work, i.e.  $W < 0$ , and its fluctuations are very large. While by quenching  $V$ , the distribution's asymmetry tends negative values (this has to deal with the entropy production), by quenching the impurity concentration, some symmetry is possible  $V > U$ .

These findings open a promising avenue to design applications for optimal work extraction, as for instance, quantum heat engines and refrigerators using various condensed matter platforms, including from nanostructures to cold atoms [17–20].

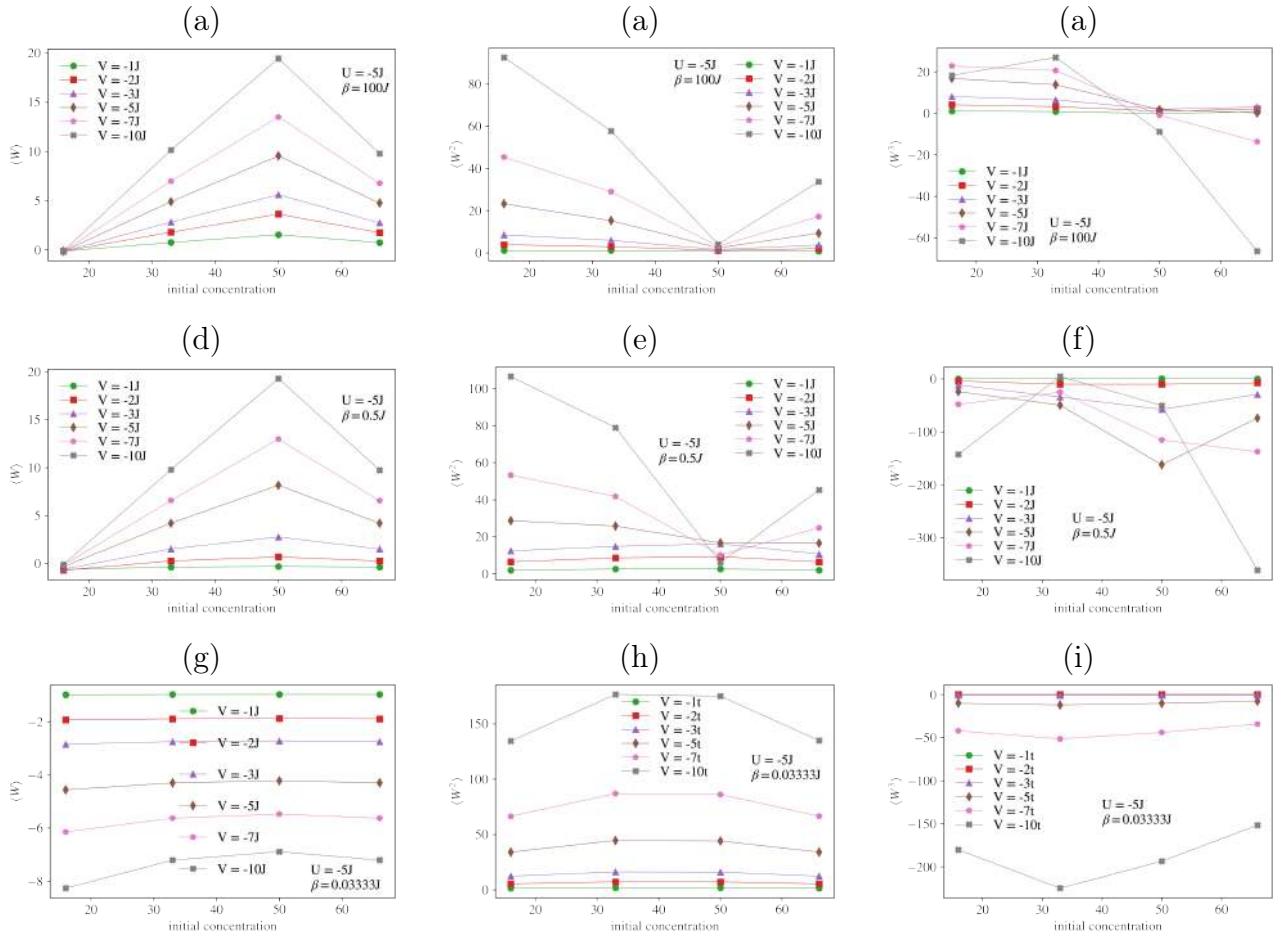


Figure 9: Average work, variance and skewness across the superfluid-Mott transition in quench protocols varying the concentration of impurities. Top row (a)-(c): low temperature. Middle row (d)-(f): intermediate temperature. Bottom row (g)-(i): high temperature.

### 1.3 Insitu thermometry for strongly correlated systems

An accurate measurement of the temperature at the nanoscales has become essential for various experiments with quantum systems, such as ultracold atomic gases [21]. The need to achieve better performance has inspired novel proposals of thermometry suiting a variety of quantum systems. Very recently, Mitchson et al [22] proposed a setup for in situ thermometry and applied it to assess the temperature of a degenerate ultracold Fermi gas. In this protocol the system in a thermal state is coupled to a qubit in time and one monitors the dephasing of this qubit to determine the so-called Quantum Fisher Information (QFI). The QFI is a key quantity to determine the precision on the measurement of the temperature and, therefore, the thermometric performance.

Inspired by this work, I have been developing a project in collaboration with Prof. Gabriel Landi (IFUSP), in which the system of interest is a finite Hubbard chain. We have been addressing the following questions: (i) if we employ an in-situ thermometry protocol to a correlated electron system, how dependent of the interactions are the bounds determining the precision in the estimate of the temperature? (ii) how to ensure a good thermometrical performance without disturbing the system across its correlated phases?, (iii) in the case of a finite correlated system, small but with a large number of degrees of freedom, is there an optimal balance between performance vs. minimal disturbance vs. correlations? Our results indicate that it is easier to achieve optimal performances at relatively short time scales in the presence of strong correlations, while systems with weak interactions are more challenging for thermometry, therefore requiring a finer tuning or design of the probe. We are currently working on a manuscript reporting these results.

The setup environment + qubit thermometer is described by the Hamiltonian

$$\hat{H} = \hat{H}_E + \hat{H}_q + \hat{H}_I, \quad (13)$$

where the first term accounts for the system  $E$  of interest, which acts as an environment for the qubit; the second term refers to the qubit  $q$  Hamiltonian; and, the third one is the interaction  $E - q$  between them.

The thermometric protocol starts from a product state  $\hat{\rho}(t = 0) = \rho_E(0) \otimes \rho_q(0)$ . At times  $t > 0$ , the total system evolves according to the Hamiltonian in eq. 13. The interaction term  $\hat{H}_I$  is built in such a way that the populations of the qubit remain unchanged in time. The qubit dephasing  $\nu(t)$ , which corresponds to off-diagonal terms of  $\rho_q(t)$ , provides the thermometric information. It is calculated as follows

$$\nu(t) = e^{-i(h_\downarrow - h_\uparrow)t} \text{Tr}_E [e^{-iH_\downarrow t} \hat{\rho}_E(0) e^{iH_\uparrow t}], \quad (14)$$

where

$$H_\sigma = \langle \sigma | \hat{H}_E + \hat{H}_I | \sigma \rangle \quad (15)$$

are the projections of the components of  $\hat{H}(t)$  containing the environment onto the qubit eigenstates  $|\sigma\rangle = \{|\downarrow\rangle, |\uparrow\rangle\}$ .

One can obtain the Quantum Fisher Information  $\mathcal{F}_T^Q$  from qubit dephasing  $v = |v|e^{i\phi}$ . Following [22], one can show that  $\mathcal{F}_T^Q$  can be expressed as the sum of two contributions

$$\mathcal{F}_T^Q = \frac{1}{1 - |v|^2} \left( \frac{\partial |v|}{\partial T} \right)^2 + |v|^2 \left( \frac{\partial \phi}{\partial T} \right)^2. \quad (16)$$

We applied this idea to study the thermometric performance in the presence of strong many-body interactions, using as the environment a homogeneous Hubbard chain. The setup

is illustrated in Fig. 10. The qubit is attached to the chain at a given site  $j$  and their interaction is described by

$$\hat{H}_I = \delta \hat{n}_j \hat{n}_{q\uparrow}, \quad (17)$$

where  $\hat{n}_{q\uparrow}$  measures the probability for the qubit to be found in its excited state  $|\uparrow\rangle$ .

We note that the choice of the site  $j$  is arbitrary. In order to assess how boundary effects affects the thermometric performance we will compare the results for attaching the qubit at the first site of the chain  $j = 0$  and in the middle  $j = L/2$ . Ideally, we would like to minimize boundary effects. We note that closer to the middle of the chain, the measurement is less sensitive to boundary effects, which in the case of Hubbard chains with open boundary conditions are important due to charge accumulation at the first and last sites.

In a strongly correlated system described by the Hubbard Hamiltonian the Coulomb repulsion  $U$  defines the characteristic energy and time scales for the system. In that sense, at a given  $U$ , the coupling  $\delta$  has to be chosen to disturb the system minimally, yet providing reasonable measurement of the QFI. The maximum of the QFI allows to identify the optimal time scales for the thermometric measurement at each temperature  $T$ . We set  $\delta = 0.2J$ , where  $J$  is the hopping parameter, and compute the normalized QFI  $\mathcal{F} = \mathcal{F}_T^Q / \mathcal{F}_{\text{th}}$ , where  $\mathcal{F}_{\text{th}} = \beta^4 (\langle H^2 \rangle - \langle H \rangle^2)$  is the thermal FI [23], which accounts for the energy variance of the Hamiltonian.

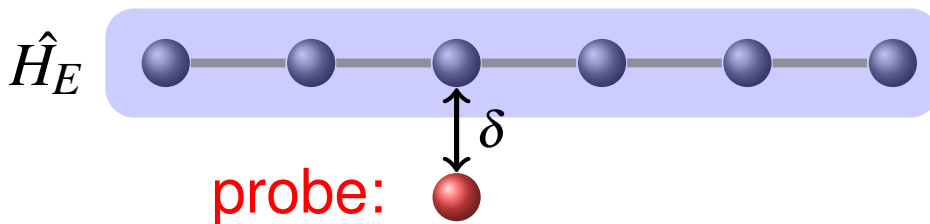


Figure 10: Sketch of the thermometric setup to study the Quantum Fisher Information in a Hubbard chain coupled to an impurity qubit.

Our main results are shown in Fig. 11, where the normalized QFI for a six site Hubbard chain as a function of the time and the temperature is shown in three coupling regimes  $U = 0.5J, 2J$  and  $5J$  for the measurement at sites  $j = 0, 2$ . The temperature of the system are shown from  $T \lesssim U$ . The color scheme depicts large values of QFI in yellow and the lowest/vanishing in blue. Overall, we note that at low temperatures, the time scales for optimal thermometric performance are relatively large  $tJ \gtrsim 200$ . For larger temperatures, however, the normalized QFI depicts a maximum at time scales below  $tJ < 100$ , and the maximum QFI is found at shorter times as the coupling  $U$  is increased. In the case of intermediate interaction,  $U \approx 2J$ , for the measure taken at  $j = 2$ , we observe that there is window of temperatures  $0.5U < T < U$  at which the QFI almost vanishes until relatively large times  $tJ < 200$ , which is different from the behavior observed in the weakly system  $U = 0.5J$ . We note that for  $U = 5J$ , the QFI indicates that the measurement is robust for all  $1 < T/J < 5$  at times shorter than  $tJ < 75$ . This enhancement of thermometry in the presence of strong coupling has been previously discussed in [24].

For typical experiments with Hubbard-like systems, for instance, in cold atom platforms, these previous results confirms the difficult in measuring the temperature with reasonable accuracy at low temperature  $T$ . The present thermometric setup should therefore be further optimized in order to address thermal scales of interest, especially in intermediate interacting regimes.

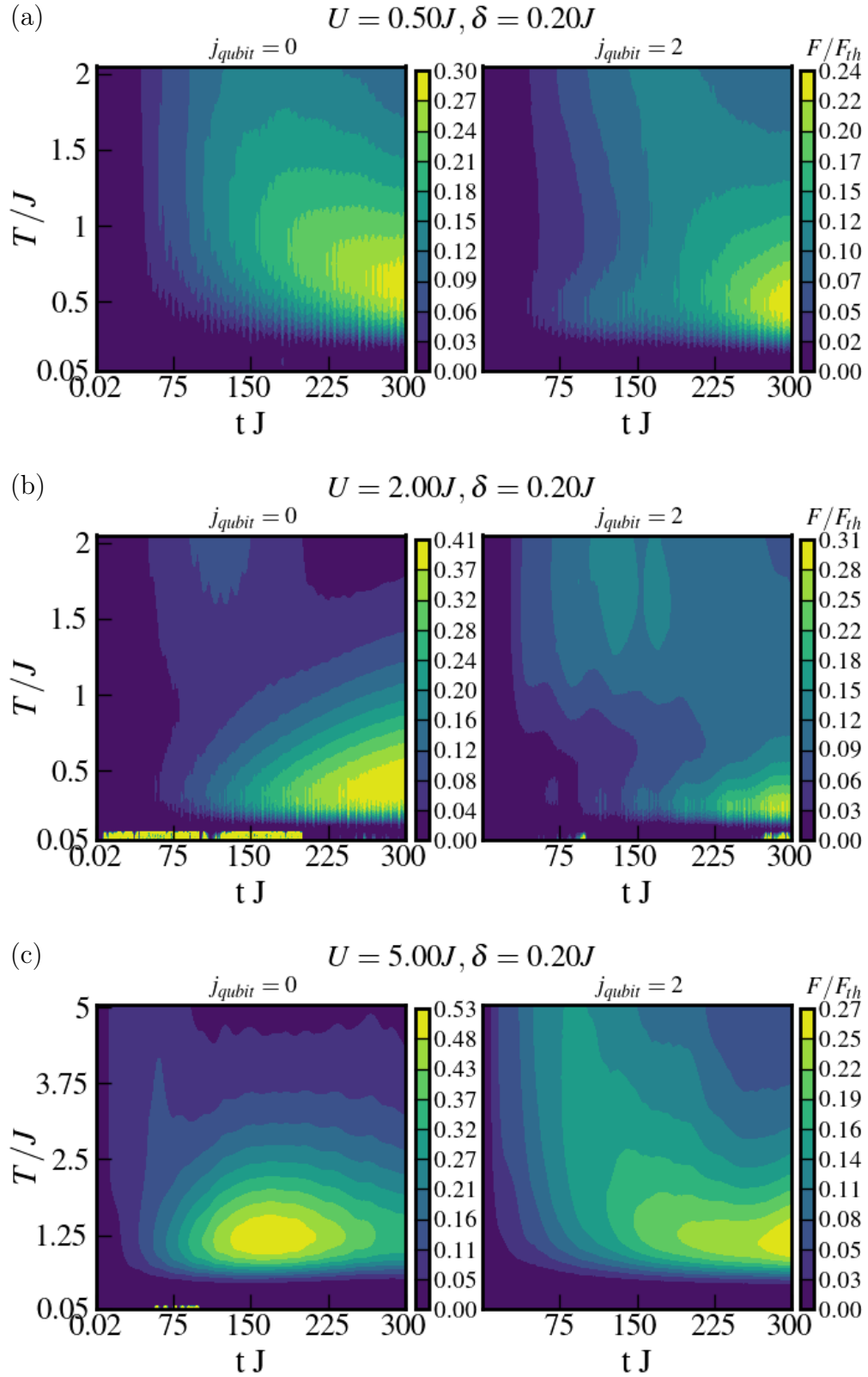


Figure 11: Normalized Quantum Fisher Information as a function of the time and the temperature  $T$  for (a) weakly coupled  $U = 0.5J$ , (b) weak insulator  $2J$  (c) strongly correlated Mott insulator  $5J$ .

## 2 Papers

- 1 K. Zawadzki, A.H. Skelt, I. D’Amico, “Approximating quantum thermodynamic properties using DFT" (in preparation)
- 2 G. A. Canella, K. Zawadzki, V. V. França, I. D’Amico, “Statistics of quantum work across the superfluid-insulator transition" (in preparation)
- 3 G. A. Canella, K. Zawadzki, V. V. França, “Effects of Concentration, Magnetization and Temperature on the Mott-Anderson Physics in one-dimensional Disordered Systems" (in preparation)
- 4 K. Zawadzki, G. T. Landi, “Disturbance versus correlation in insitu thermometry" (in preparation)
- 5 K. Zawadzki, A. Nocera, A. E. Feiguin, “A time-dependent scattering approach to core-level spectroscopies" [arXiv:2002.04142](https://arxiv.org/abs/2002.04142) [cond-mat.str-el]

## 3 Events

### 3.1 Presentations

- 1 K. Zawadzki, A. Nocera, A. E. Feiguin, “Time-dependent scattering approach to compute RIXS spectra" *APS March Meeting 2021 Session Y22: First-Principles Modeling of Excited-State Phenomena in Materials VII: X-Ray Spectroscopy*, Virtual; USA. March 2021  
\*Award: APS-FECS Early Career minigrant covering the full costs of attendance.
- 2 K. Zawadzki, , “Simulating spectroscopies beyond perturbation theory: an exact numerical approach", *Encontro de Outono da Sociedade Brasileira de Física 2021 Theory and Simulation II*, Online; Brazil. June 2021
- 3 K. Zawadzki, “Time and momentum resolved spectroscopies made easy with tDMRG” *Correlations in Novel Quantum Materials, Max Planck Institute for Solid State Research Poster session*, Online; Stuttgart, Germany. June 2021
- 4 G. A. Canella, K. Zawadzki, V. V. França, I. D’Amico, “Statistics of quantum work across the superfluid-insulator transition" *Recent advances in quantum thermodynamics with a focus on many-body interactions Session 2*, Online; UK. July 2021

### 3.2 Attendance

- 1 *A mini-course on Quantum-Information Thermodynamics, Quantum Thermodynamics and Quantum Transport (QT<sup>2</sup>) group*; Brazil. November 2020
- 2 *Encontro de Outono da Sociedade Brasileira de Física 2020*, *Sociedade Brasileira de Física*; Brazil. November 2020
- 3 *Workshop II: Tensor Network States and Applications. Institute for Pure and Applied Mathematics (IPAM)*, Online; California, USA. April 2021

- 4 *International Workshop Quantum Many-Body Dynamics: Thermalization and its Violations*. Center for Theoretical Physics of Complex Systems Institute for Basic Science, Online; Korea. May 2021

## 4 Outreach and Volunteering

Before joining ICTP, I have been involved with the organization of a series of online seminars, called [Quantum Matter Seminars](#), conceived by Prof. Adrian Feiguin (Northeastern University) in June 2020. I co-organized this seminar series during the first semester of 2021.

Since 2018, I have been collaborating with the group [Pyladies São Carlos](#). Pyladies is a global community whose ultimate goal is include more women in technological careers and provide them educational and training resources by means of which they can develop professionally. In Sao Carlos, the Pyladies chapter is organized mainly by students (both at undergrad and graduate levels) at the University of Sao Paulo (USP) and Federal University of Sao Carlos (UFSCar). My duties in this group include training activities (courses and workshops) and the creation content for social media (mainly posts focused on teaching python tools).

In 2021, I started to collaborate with *Minas do IFSC*, a group created by Prof. Tereza Mendes at the Sao Carlos Institute of Physics (IFSC-USP), where I obtained my BSc, MSc and PhD in Physics. The aim of this group is to mentor female undergraduate students at IFSC and help them to succeed during their studies.

## 5 Examination committees

- SIFSC 2011, Yvonne Primerano Mascarenhas Award (YPM), undergraduate research projects. Sao Carlos Institute of Physics at the University of Sao Paulo (IFSC-USP). September 2021.
- Masters dissertation: Mariana Afeche Cipolla. Institute of Physics at the University of Sao Paulo (IF-USP). Supervisor: Gabriel T. Landi. September 2021

## References

- [1] J. Goold, M. Huber, L. del Rio, and P. Skrzypczyk. The role of quantum information in thermodynamics - a topical review. *J. Phys. A*, 49(143001), 2016.
- [2] Sai Vinjanampathy and Janet Anders. Quantum thermodynamics. *Contemporary Physics*, 57(545), 2016.
- [3] J. Millen and A. Xuereb. Perspective on quantum thermodynamics. *New J. Phys.*, 18(011002), 2016.
- [4] J. M. R. Parrondo, J. M. Horowitz, and T. Sagawa. Thermodynamics of information. *Nat. Phys.*, 11(131), 2015.
- [5] P. Luizzo-Scorpo, L. A. Correa, R. Schmidt, and G. Adesso. Thermodynamics of quantum feedback cooling. *Entropy*, 18(48), 2016.

- [6] A. H. Skelt, K. Zawadzki, and I. D’Amico. Many-body effects on the thermodynamics of closed quantum systems. *Journal of Physics A: Mathematical and Theoretical*, 52(48):485304, 2019.
- [7] N. A. Lima, M. F. Silva, L. N. Oliveira, and K. Capelle. Density functionals not based on the electron gas: Local-density approximation for a luttinger liquid. *Phys. Rev. Lett.*, 90:146402, Apr 2003.
- [8] J. P. Coe, I. D’Amico, and V. V. França. Uniqueness of density-to-potential mapping for fermionic lattice systems. *EPL (Europhysics Letters)*, 110(6):63001, 2015.
- [9] Andreas Osterloh, Luigi Amico, Giuseppe Falci, and Rosario Fazio. Scaling of entanglement close to a quantum phase transition. *Nature*, 416(6881):608–610, 2002.
- [10] Daniel Larsson and Henrik Johannesson. Single-site entanglement of fermions at a quantum phase transition. *Phys. Rev. A*, 73:042320, Apr 2006.
- [11] V. V. França and K. Capelle. Entanglement in spatially inhomogeneous many-fermion systems. *Phys. Rev. Lett.*, 100:070403, Feb 2008.
- [12] V. V. França and K. Capelle. Entanglement of strongly interacting low-dimensional fermions in metallic, superfluid, and antiferromagnetic insulating systems. *Phys. Rev. A*, 74:042325, Oct 2006.
- [13] GA Canella and VV França. Mott-anderson metal-insulator transitions from entanglement. *arXiv preprint arXiv:2105.12529*, 2021.
- [14] G.A. Canella and V.V. França. Entanglement in disordered superfluids: The impact of density, interaction and harmonic confinement on the superconductor–insulator transition. *Physica A: Statistical Mechanics and its Applications*, 545:123646, 2020.
- [15] Eric G. Arrais, Diego A. Wisniacki, Augusto J. Roncaglia, and Fabricio Toscano. Work statistics for sudden quenches in interacting quantum many-body systems. *Phys. Rev. E*, 100:052136, Nov 2019.
- [16] K. Zawadzki, R. M. Serra, and I. D’Amico. Work-distribution quantumness and irreversibility when crossing a quantum phase transition in finite time. *Phys. Rev. Research*, 2:033167, 2020.
- [17] Xiaoguang Luo, Hexin Zhang, Dan Liu, Nannan Han, Dong Mei, Jinpeng Xu, Yingchun Cheng, and Wei Huang. Efficiency at maximum power of thermoelectric heat engines with the symmetric semiconductor superlattice. *Physica E: Low-dimensional Systems and Nanostructures*, 129:114657, 2021.
- [18] Andreas Hartmann, Victor Mukherjee, Wolfgang Niedenzu, and Wolfgang Lechner. Many-body quantum heat engines with shortcuts to adiabaticity. *Phys. Rev. Research*, 2:023145, May 2020.
- [19] Giovanni Barontini and Mauro Paternostro. Ultra-cold single-atom quantum heat engines. 21(6):063019, jun 2019.
- [20] François Damanet, Eduardo Mascarenhas, David Pekker, and Andrew J Daley. Reservoir engineering of cooper-pair-assisted transport with cold atoms. 21(11):115001, nov 2019.

- [21] Francesco Giazotto, Tero T. Heikkilä, Arttu Luukanen, Alexander M. Savin, and Jukka P. Pekola. Opportunities for mesoscopies in thermometry and refrigeration: Physics and applications. *Reviews of Modern Physics*, 78(1):217–274, 3 2006.
- [22] Mark T. Mitchison, Thomás Fogarty, Giacomo Guarnieri, Steve Campbell, Thomas Busch, and John Goold. In Situ Thermometry of a Cold Fermi Gas via Dephasing Impurities. *Physical Review Letters*, 125(8):080402, 8 2020.
- [23] Karen V. Hovhannisyán, Mathias R. Jørgensen, Gabriel T. Landi, Álvaro M. Alhambra, Jonatan B. Brask, and Martí Perarnau-Llobet. Optimal quantum thermometry with coarse-grained measurements. *PRX Quantum*, 2:020322, May 2021.
- [24] Luis A. Correa, Martí Perarnau-Llobet, Karen V. Hovhannisyán, Senaida Hernández-Santana, Mohammad Mehboudi, and Anna Sanpera. Low-temperature thermometry can be enhanced by strong coupling. *Physical Review A - Atomic, Molecular, and Optical Physics*, 96:062103, 2017.